Classification, Seasonality and Persistence of Low-Frequency Atmospheric Circulation Patterns

ANTHONY G. BARNSTON

Climate Analysis Center, NMC/NWS/NOAA, Washington, DC 20233

ROBERT E. LIVEZEY*

Goddard Laboratory for Atmospheres, NASA/Goddard Space Flight Center, Greenbelt, MD 20771

(Manuscript received 27 June 1986, in final form 4 November 1986)

ABSTRACT

Orthogonally rotated principle component analysis (RPCA) of Northern Hemisphere 1-month mean 700 mb heights is used to identify and describe the seasonality and persistence of the major modes of interannual variability. The analysis is detailed and comprehensive, in that 1) a high resolution, approximately equal-area 358-point grid is used for the virtually maximum possible 35-year period of record, 2) a positive bias in the NMC data base in the early 1950s in the subtropics is largely eliminated for the first time, and 3) homogeneous, separate analyses of each month of the year are carried out, detailing the month-to-month changes in the dominant circulation patterns.

Winter results are similar to those of other recent RPCA and teleconnection studies except that some less obvious patterns are identified and further detail of the better-known patterns is provided. Two north–south dipole patterns are found over the Pacific Ocean (West Pacific Oscillation and East Pacific pattern) and over the Atlantic Ocean (North Atlantic Oscillation and East Atlantic pattern); two uncorrelated phases of 3-center, approximately east–west wave trains are found over the Eurasian continent (Eurasian Type 1 and Eurasian Type 2 patterns) and North American continent (Pacific/North American and Tropical/Northern Hemisphere patterns) and a Siberian north–south dipole emerges (Northern Asian pattern).

The strongest summer pattern is also the strongest winter pattern—the North Atlantic Oscillation, which systematically contracts northward in summer and expands southward in winter, being the only pattern found for every month of the year. Another strong summer pattern, named Subtropical Zonal, is a north–south dipole of great zonal extent at low latitudes. A single-center Asian summer pattern is also found. Two other regular patterns are found during transition seasons.

An evaluation of the intermonthly and interseasonal persistence of the patterns shows that many of the strong winter patterns have statistically significant persistence in the middle of their active periods, and the Subtropical Zonal summer pattern shows considerable interannual, as well as intermonthly and interseasonal persistence.

The robustness of the RPCA results is examined through consistency with results of other studies and of adjacent month solutions within this study, and by replicating the results using 3-month and 10-day means of 700 mb height. (Results using 10-day means point the way to use of a larger sample without noticeably obscuring the low-frequency signal.) Moreover, the analyses are repeatedly rerun withholding different sets of years from the record, and results are objectively compared with those using the full 35-year record. The conclusion from all considerations is that the RPCA method provides a physically meaningful, as well as statistically stable product with the simplicity of teleconnection patterns but with pattern choice and depiction superior to those of the teleconnection method.

1. Introduction

The behavior of the quasi-stationary, upper-air planetary-scale circulation is of considerable interest to meteorologists for a variety of reasons. One practical reason, and the one which motivates this work, is that it is strongly coupled with the short-term climate fluctuations at the surface (see Klein, 1983, for example), which we hope to predict. To better understand this flow—its characteristic nature, temporal behavior, and relationship to the surface climate—it is desirable to identify and objectively classify its preferred (i.e., persistent or recurring) modes and define their active periods of the year.

Two approaches have been used in recent empirical studies to do this for low-frequency variability (i.e., variability of the planetary waves on time scales of several weeks upward to several years). The first, the teleconnection method, obtains temporal correlations in a meteorological parameter between one given geographical location and all others in the domain. This exercise is repeated using every possible point as the base point. The locations producing the highest amplitude, best defined versions of uniquely configured correlation fields (called teleconnection patterns) are accepted as the "centers of action" of the low frequency variability. A teleconnection pattern typically includes two to four main centers of action (including that of the base point), with the strongest remote correlations being negative and occurring between points in the base center and those in an adjacent center located

* Present affiliation: Climate Analysis Center, NMC/NWS/NOAA, Washington, DC 20233.

Unauthenticated | Downloaded 08/21/22 12:56 PM UTC

some 2500–6000 km distance away. It is the strength of this negative correlation that is used in deciding whether or not the pattern produced for any given base point location is to be accepted as one of the major teleconnection patterns. As will be shown below, this criterion in general does not lead one to choose the most representative set of patterns; nor is it straightforward to define the relative importance of centers within a pattern or the temporal evolution of patterns.

Extensive documentation of Northern Hemisphere winter teleconnection patterns of sea level pressure and 500 mb height is provided by Wallace and Gutzler (1981, hereafter referred to as WG). A later study using winter 700 mb heights (Esbenson, 1984, hereafter E) found many of the same patterns and provided additional information about the time scale of their fluctuations. Blackmon et al. (1984a, 1984b) also examined the time scale dependence of circulation patterns, and suggested that the longer time scale patterns (over one month) are mostly fixed north–south dipoles over oceans while those having intermediate time scales (10–30 days) are zonally oriented curved ray paths that shift with reference point. In earlier teleconnection work by O'Connor (1969) and Namias (1981), no attempts were made to identify preferred circulation patterns. Instead, patterns created by all possible base points were mapped rather than only those producing the best defined correlation fields, resulting in teleconnection atlases.

A second method of defining the low-frequency circulation patterns is that of rotated principle component analysis (RPCA), whereby the eigenvectors of the cross-correlation (or cross-covariance) matrix, often derived from the time variations of the grid-point values of the meteorological parameter, are individually scaled according to the amount of total data variance they explain (making a principal component analysis), and then linearly transformed (i.e., rotated) under certain constraints to obtain the major circulation patterns. The constraints take advantage of several apparent properties of the large-scale quasi-stationary upper-air flow patterns to produce physically meaningful, distinct, and statistically robust solutions. The flow properties that make the analysis so appropriate are 1) the regionality of the low-frequency circulation modes (each occupies only 15%–50% of the extratropical hemispheric domain) and 2) the fact that they are not necessarily spatially orthogonal to each other but seem to be approximately temporally uncorrelated.

To see why the choice of rotation constraints is so critical, the examples of WG and Horel (1981, hereafter referred to as H81) are instructive. In WG, unrotated eigenvectors of the SLP and the 500 mb height data were computed and found not to be particularly reflective of the teleconnection patterns. They were less meteorologically interpretable, involved much larger areas of the hemisphere (containing five or more centers of action), and were less statistically stable when a different period of record was used than the teleconnection patterns. All of these properties are a consequence of the eigenvector analysis; each succeeding eigenvector computed explained less variance and was constrained to be spatially and temporally orthogonal to all those preceding it. This procedure tends to produce patterns that are global in extent, progressively smaller in scale, and nonrobust. However, upon rotation of the WG eigenvectors, H81 found the solutions to be simpler in structure, more physically reasonable, and more similar to the WG teleconnection patterns.

These same issues concerning RPCA as well as the question of its robustness are extensively discussed by Richman (1986). His Monte Carlo simulations addressing the statistical stability of unrotated and rotated principal components confirm that the latter are much less vulnerable to sampling error than the former. This has also been the experience of Horel (1984) and Hsu and Wallace (1985, hereafter referred to as HW). We will examine the robustness of our RPCA patterns of geopotential height from a number of standpoints, including internal consistency of our results and sample sensitivity tests. We will likewise compare our results using an orthogonal (varimax) rotation algorithm (Kaiser, 1958, 1959) with results of a similar analysis using an oblique (Harris–Kaiser II, B'B; Harris and Kaiser, 1964) rotation algorithm (Lebow and Toldalagi, 1985; hereafter denoted by LT), as well as to 500 mb patterns associated with RPCA of sea level pressure (HW). The single instance we are aware of in which RPCA results were apparently nonrobust for an upper-air, low-frequency pattern analysis is in H81, where there is now little doubt with the benefit of hindsight that data problems, rather than the RPCA method, caused the inconsistencies between the results of a 15-year analysis and a 30-year analysis. More will be said about this in section 4b. One outcome of the present study is a demonstration that the RPCA method applied to appropriately gridded, relatively problem-free, hemispheric geopotential height data not only yields a detailed and robust description of teleconnection counterparts, but also produces other patterns likely to be overlooked in the teleconnection screening procedure. In this context, RPCA patterns seem to form the most suitable basis for empirical climate studies where circulation structure is important; i.e., specification studies, prediction studies, etc.

There are several reasons why RPCA has not been readily accepted as the most powerful approach for analysis of the low-frequency planetary waves. Teleconnections are conceptually simpler (i.e., less removed from the realm of the original data), and the favorable characteristics of RPCA (completeness, interpretability, stability) have not yet been fully acknowledged. Some researchers still associate RPCA with the unrotated eigenvector patterns, which are mathematically designed exclusively to maximize variance accounted for in each succeeding vector, and not necessarily to extract the components as individual portions of variance belonging specifically to the empirically distinct inter-

Unauthenticated | Downloaded 08/21/22 12:56 PM UTC

correlational complexes in the dataset. Because RPCA is designed to extract components from the unrotated PCs in the latter way, it is a more desirable approach than that of teleconnections for the following reasons. The amplitudes of the RPCA centers are accurate depictions of their relative physical strengths in the patterns, whereas the teleconnection center containing the base point always has an artificially inflated magnitude in comparison with the remote centers, and the more remote features of the major patterns are influenced by a multiplicity of responses that are separable when using RPCA. This is because a teleconnection pattern is a correlation field, and thus a "blind" net result of the multiple underlying constituent correlational entities. The amount of variance explained by a teleconnection pattern is difficult to determine, whereas that of an RPC is exactly specifiable.

Another major drawback in teleconnections is that they are usually chosen on the basis of the strength of the primary negative correlation with the base point, neglecting other relevant information, such as the areal coverage of the pattern. The choice of base point position must be partly subjective, as when a north–south dipole remains nearly equally strong as the base point is moved zonally. One consequence of this problem is omission of patterns associated with certain base point locations that do not provide very strong primary negative correlations but do produce patterns that represent unique, physically based correlational complexes. An example of such an oversight will be presented in section 3.

Finally, the set of RPCA patterns form a complete basis for a substantial portion of the original dataset's variance, and each pattern has an associated temporal history (the principal components). As such, they can be used quantitatively in a broad range of empirical studies and applications, such as the lag-correlational analyses presented below (3e) to explore pattern persistence and transition. On the other hand, many direct uses of composites of teleconnection patterns have been necessarily subjective.

As stated in H81, RPCA is not inherently guaranteed to represent the underlying physical relationships. In order for such representation to occur, 1) the dataset must contain a sufficient strength of the subject signal(s) as compared with confounding sources of variability (e.g., "noise"), and 2) the signal must have simple structure so that a rotation criterion such as varimax will point the axis of each successive mode in the most appropriate direction in hyperspace with little ambiguity. All indications (including teleconnections) appear to characterize hemispheric low-frequency geopotential height variations as having simple structure, and results of the present study will further confirm this hypothesis.

The main subject of this paper is not statistical or methodological, but substantive. Using 1-month mean Northern Hemispheric densely gridded 700 mb heights as the primary (but not exclusive) data, the major low-frequency circulation patterns for each of the 12 months are defined using RPCA. The consistency of the patterns among adjacent months, the evolution of their structure over the course of the year, and the statistical stability of each of the patterns themselves are examined. Patterns are compared with those produced using other averaging periods. Results are closely compared with those of the major recent teleconnection and RPCA studies of the low-frequency circulation, and an up-to-date (as of 1986) account of the major modes of low-frequency atmospheric variability and their seasonality is presented. The persistence of the patterns between adjacent 1-month and 3-month periods also is examined, and the subject of transitions from one atmospheric response to another is discussed.

In section 2, the details of the 700 mb height data, the grid and the RPCA are given. All major results are presented in section 3: descriptions of the circulation patterns, their seasonality and persistence, and their correspondence to patterns found in other studies. This section might be described as encyclopedic in nature and length; many of the subsections or detailed pattern descriptions that might be of interest to one or another group of specialists or regionalists will not necessarily be of general interest. Consequently, much of the narrative in section 3 can be skipped without loss of continuity. Further guidance in this matter will be provided the reader in section 3. In section 4, the robustness and consistency of the results (with respect to other studies and within the present study) are evaluated to ensure that the degree of degeneracy found in unrotated PCs (North et al., 1982) is not evidenced in the RPCs. Conclusions are found in section 5.

2. The data and the rotated principal component analysis

The data used in this study were derived from the twice-daily Northern Hemisphere 700 mb height data from 1950 through 1984 from the National Meteorological Center (NMC). The data are given at 541 grid points, with 36 points on each of the 15 5-degree-apart latitude circles between and including 15°N and 85°N, plus one point at 90°N. The longitudes are offset by 5° on successive latitude circles such that the points form diamonds rather than rectangles.

Before converting to a more suitable grid for our analyses, monthly mean heights at each of the 541 points were computed by averaging the heights of the available twice-daily values. Brief periods of missing daily data were infrequent; temporal interpolation using data of adjacent days was carried out in such instances. Mean heights for two other averaging periods were formed in a similar manner: 10-day means and 3-month (seasonal) means. Consecutive 10-day means were centered one day apart, forming 30 means per month, while consecutive seasonal means were centered one month apart, creating 12 seasons per year.

Because the 541-point grid has more points per unit

Unauthenticated | Downloaded 08/21/22 12:56 PM UTC

area near the pole than at the lower latitudes, a more nearly equal area grid was designed in order for the eigenvector loading patterns to become physically representative following rotation (Karl et al., 1982). A more uniform gridding density was achieved by retaining 36 points per latitude circle from 20° to 55°N (15°N was discarded because of missing data in the early part of the record), using 24 points at 60° and 65°N (requiring spatial interpolation for half of the points), 18 points at 70°N, 12 at 75°N, 9 at 80°N, and 4 at 85°N with no point at the pole. In addition to discarding data at 15°N, points at 20°N from 20°E to 90°E were omitted because of a lack of 1950 data. Himalayan grid points were also rejected because 700 mb heights are largely fictitious there. The fact that data coverage is not complete from equator to pole is unimportant to the subsequent analysis, because RPCA is quite insensitive to the data domain (Richman, 1986). The resulting well-resolved 358-point grid is shown in Fig. 1.

A thorough screening of the data behavior at all grid points in the 1950–84 period uncovered a noticeable positive bias, especially in summer, in the early and middle 1950s in the Caribbean and North Africa. This problem, which was noted in the summer RPCA results in H81, may have been caused by a change in the NMC analysis procedure. Data at 16 of the 358 grid points (indicated in Fig. 1) were edited to largely eliminate the bias, affecting the RPCA results in summer quite noticeably but at other times of year only negligibly. The details of the bias correction are provided in appendix A.

To ensure the inclusion of the systematic but low variance lower latitude variations in the results, a correlation rather than covariance matrix was used in eigenvector computations. Intercorrelations among the grid points were computed over the 35-year sample for each month. The ones on the diagonal of the matrix were retained rather than replaced with estimates of communalities; i.e., principal component analysis, not common factor analysis, was performed. (This distinction is not crucial here, because the communalities would be close to unity owing to the high temporal correlations of 700 mb height among adjacent grid points.) Note that different time periods were not pooled for each RPCA. For example, the January analysis contained only the 35 Januaries on record; no concatenated or overlapping periods, such as means for December, January and February, were used to bolster the "January" sample size. This constitutes a considerable departure from previous practice (see upper portion of appendix B) and reflects our confidence in the sampling stability of the RPCA and our reluctance to obscure important month-to-month changes in the set of patterns and in patterns replicated in adjacent months.

Most of the unrotated eigenvector spatial patterns contained strong features throughout the hemisphere (similar to Fig. 27 in WG), which are counter to the more regional circulation patterns our experience suggests are the physical responses. Increased physical interpretability was achieved by rotating the principal component loading vectors (i.e., eigenvectors multiplied by the square roots of their eigenvalues) using the orthogonal varimax rotation algorithm. The resulting RPCA loading patterns, as expected, contained many near-zero elements and a relatively small number of highly positive or negative elements—i.e., regionally focused patterns. Only the first ten unrotated modes were used in all rotation analyses. This truncation point included about 80% of the original variance in winter and 70% in summer. Table 1 lists the percentages of total variance explained by each unrotated and rotated principal component for the 1-month averages of 700 mb height for each of the 12 months.[1] In effect, the preliminary PCA is being used as a filter before the final rotation. The principal concern with this procedure is that important signal not be thrown out with the discarded modes. For every month in the study, the truncation point was close to (but in no case included more modes than) the Guttman criterion (Guttman, 1954), and the eigenvalue curve in the vicinity of the point relatively flat. Both facts together suggest that not much signal was excluded with the truncation. To check this, 11 modes were rotated instead of 10 with little apparent change in results. Further evidence of the reproducibility of results is presented in section 4.

A note on the presentation of RPCA patterns is necessary. All figures are in "anomaly" form, because the eigenvectors are computed from the correlation coefficients. The values are scaled to be correlations between the 700 mb heights at a given grid point and the principal component time series of the mode in question. Furthermore, signs of the centers are arbitrary such that the polarity of a pattern can be regarded either as shown or in reverse. Therefore, the RPCA maps can be interpreted similarly to teleconnection pattern maps.

3. Results

In this section the major circulation patterns produced from the RPCA of 1-month mean 700 mb heights are summarized, first for the cold part of the year and then for the warm and transition seasons. Results of the same RPCA applied to 3-month and 10-day mean heights are also presented for comparative purposes. Those for 3-month mean heights can be found in appendix E. The patterns to be displayed here have fared satisfactorily or better on the stability/robustness estimates to be described in section 4.

One obvious test of stability is the occurrence of the

[1] The percentages of original variance captured in the aggregate of the first 10 modes varied among grid points, because some of the points participated more actively than others in the PCA-extracted patterns. These interpoint differences were not normalized prior to rotation.

Unauthenticated | Downloaded 08/21/22 12:56 PM UTC

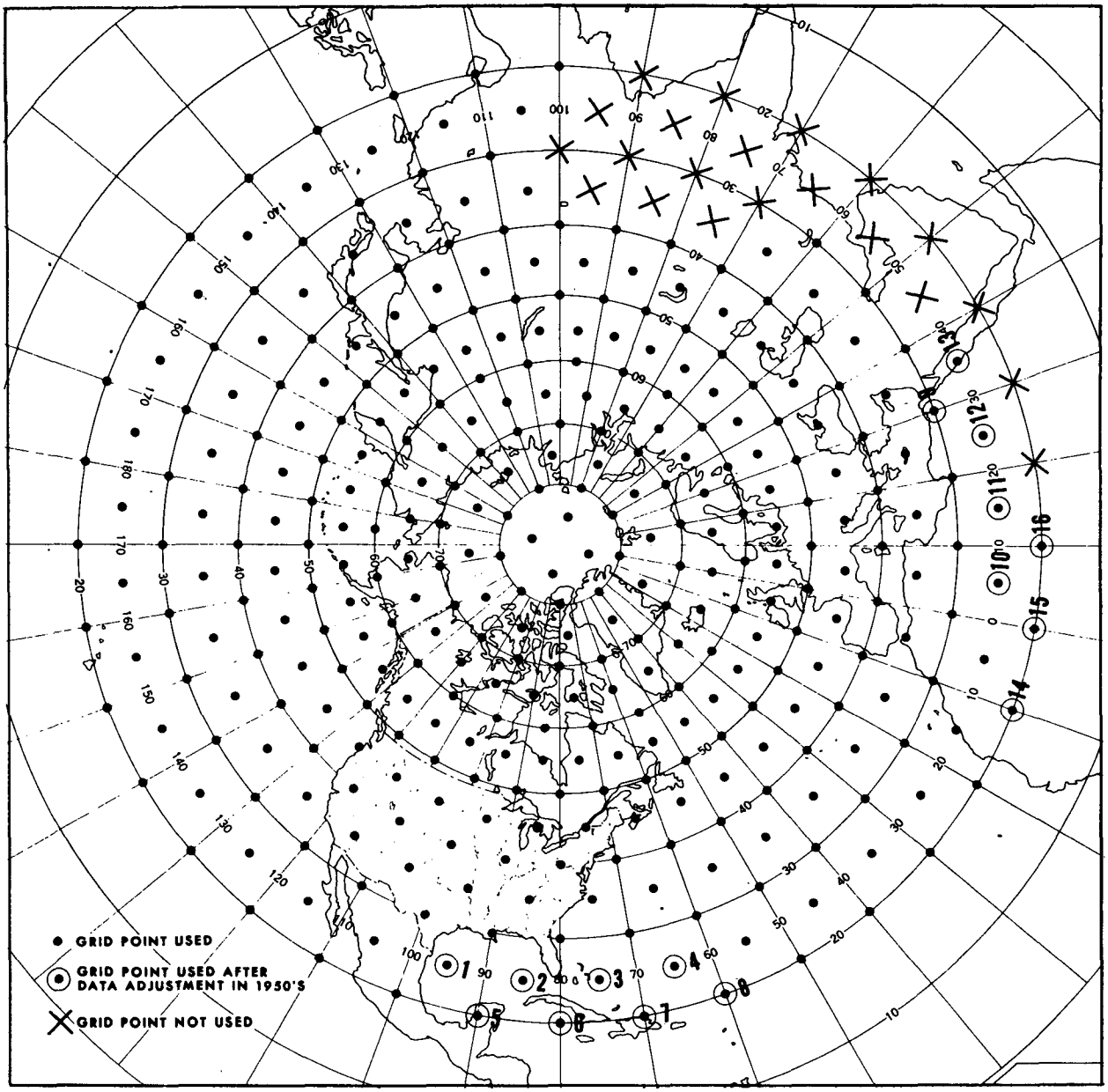

FIG. 1. The 358-point Northern Hemisphere grid used for input of time-averaged 700 mb data to the rotated principal component analysis.

same pattern in adjacent, independent monthly analyses. This is because adjacent monthly means are only very weakly correlated with each other (van den Dool and Livezey, 1984). Patterns that occur unambiguously in three successive months are unquestionably coherent physical modes. This is the case for all of the patterns to be highlighted here.[2] Such pattern replication was largely assessed by eye with the aid of pattern correlations between all patterns in adjacent months. This was followed by the robustness tests detailed in section 4c. A pattern that only marginally satisfied these tests was usually accepted for the month in question if one or both of the neighboring months had robust versions of the same pattern, whereas it was rejected in the absence of adjacent month support. In the former case, acknowledging and tabulating the pattern assists the process of tracing the seasonal waxing and waning of the mode's importance in the general circulation.

As the winter patterns are described and illustrated by figures in this section, they also are compared with similar patterns found in the teleconnection studies of WG and E, and with the RPCA studies of H81, LT,

[2] In three cases some mixing or separation is present for one of the three months, but the pattern is clearly identifiable.

Unauthenticated | Downloaded 08/21/22 12:56 PM UTC

TABLE 1. Percent of variance explained by each of the first 10 unrotated (Unr) and rotated (Rot) principal components of 1-month mean 700 mb heights.

	Jan		Feb		Mar		Apr		May		Jun		Jul		Aug		Sep		Oct		Nov		Dec	
Mode	Unr	Rot	Unr	Rot	Unr	Rot	Unr	Rot	Unr	Rot	Unr	Rot	Unr	Rot	Unr	Rot	Unr	Rot	Unr	Rot	Unr	Rot	Unr	Rot
1	18.2	11.1	18.0	13.2	18.2	15.4	16.1	11.1	12.9	10.8	11.4	9.5	11.4	9.6	13.1	10.1	11.8	9.0	13.0	10.6	13.0	10.2	14.6	11.1
2	14.8	10.8	12.0	12.3	10.9	8.0	9.7	9.5	11.2	9.1	10.4	8.8	9.7	7.9	11.1	8.8	10.1	9.0	10.8	8.9	12.1	9.9	11.6	9.7
3	11.2	9.8	11.3	10.4	10.8	7.7	8.8	8.3	9.2	7.8	10.0	7.8	8.7	7.5	9.2	7.8	10.0	8.1	10.0	8.7	9.1	9.4	10.9	8.9
4	9.3	9.8	9.5	7.8	8.9	7.4	7.2	7.4	7.9	7.4	7.7	7.6	7.3	6.8	6.8	7.1	9.0	7.8	7.4	8.3	8.1	8.0	10.2	8.6
5	7.0	8.3	6.9	7.7	7.4	7.3	7.0	7.0	6.9	7.0	5.8	7.5	6.5	6.3	6.3	7.0	6.4	7.6	6.8	7.4	7.8	8.0	7.5	8.3
6	5.3	8.0	5.9	7.4	5.9	7.2	6.1	6.6	6.0	6.7	5.4	6.6	6.0	6.2	5.7	6.4	5.8	7.0	6.2	7.3	6.4	7.9	6.5	7.9
7	4.5	7.7	5.6	7.0	5.0	7.1	5.4	6.5	5.3	6.7	4.9	5.7	5.2	6.1	5.3	6.3	5.6	6.5	5.9	6.5	5.6	6.4	5.3	6.7
8	4.3	5.8	4.2	5.2	4.5	7.0	4.8	6.4	4.5	5.7	4.5	5.1	4.6	6.0	4.8	6.3	4.6	5.8	5.0	6.3	5.1	5.8	4.6	6.5
9	3.6	5.2	3.6	4.7	3.9	6.3	4.4	5.4	3.8	5.3	4.3	4.9	4.4	5.9	4.1	5.4	4.3	5.4	4.2	5.1	3.9	4.9	3.8	6.3
10	3.2	5.0	2.9	4.2	3.7	5.8	4.1	5.4	3.6	4.8	4.0	4.8	4.0	5.5	3.6	5.0	3.6	5.1	3.2	3.4	3.8	4.3	3.1	4.1
Total	81.3		79.8		79.1		73.6		71.4		68.3		67.8		70.1		71.3		72.4		74.8		78.1	

and HW. A "master chart" delineating the correspondences between our patterns and those of the five other studies is provided in appendix B. It is designed to facilitate comparison of our figures with those showing similar patterns in the other articles. The summer results can only be compared with LT and the 30-year analysis of H81, and spring and fall results only with LT. Their respective "master charts" constitute appendices C and D.

All of the circulation patterns considered to be of meteorological interest in the five other studies appeared in our RPCA loading patterns—many on a one-to-one basis with theirs but some as parts or combinations thereof. Some of the transition season and summer patterns to be described below have not until now been formally documented.

In Table 2, the seasonal life cycles of all the acceptable 1-month RPCA patterns (denoted by 2- or 3-letter abbreviations) to be described now are shown, indicating which component (or mode) number (1 being the mode explaining the most variance, 10 the least) was occupied by each pattern for each of its active months. As indicated in Table 2, nine cold season patterns, three essentially warm season patterns and three transition season patterns were identified, with one pattern (NAO) being counted in all three seasonal categories. The month showing a mode number enclosed by hyphens for any given pattern is the month with a highly representative or prototypical example of that pattern. (It often, but not invariably, is also the month for which the pattern has greatest statistical robustness; this issue will be examined in section 4.) For the stronger, more stable patterns that have long annual life cycles, any of several months could serve equally well as the prototype. Superscripts indicate that a second identifiable pattern is also present in the RPCA result, the superscript content identifying the pattern. Single modes showing two patterns combined or blended are regarded as acceptable representations of both if the characteristics conform to those exhibited in cases where each pattern occupies its own mode. (While RPCA is considerably less vulnerable to "mixing" problems than unrotated PCA, such problems will still occur occasionally in weak signal, "noisy" situations. Using the orthogonal varimax rotation algorithm when the natural atmospheric circulation patterns are not always perfectly temporally orthogonal can also cause mixing in some instances.) Finally, parentheses indicate that the pattern is not in strict agreement with the description below, but that its identity is nonetheless strongly suggested.

For every pattern described in sections 3a–c, at least one map, a table entry in appendix B, C or D, and word descriptions of both are provided. The word descriptions are redundant, but essential to the specialist and for complete exposition. Consequently, almost all of the narrative in these sections can be skipped without loss of continuity through a review of Figs. 2–14 and appendices B–D. Exceptions to this are the following:

Unauthenticated | Downloaded 08/21/22 12:56 PM UTC

TABLE 2. Mode numbers of patterns associated with 1-month mean 700 mb height rotated principal components during their active periods. See text for explanation of symbols.

	All	Cold season								Warm		Transition	
Month	NAO	PNA	WPO	TNH	NA	EU1	EU2	EA	EP	SZ	AS	NP	PT
Jan	-1-	2	3	-4-	-5-	6	-7-	8	10				
Feb	2^{EU2}	-1-	3	6	7	(10)	2^{NA0}	-4-	-8-				
Mar	1	3	5^{SZ}		7^{EU1}	$(7)^{NA}$	6	9	4	5^{WPO}			
Apr	(3)	6	2^{SZ}			7		8		2^{WPO}		1	9
May	1		2			6						-3-	-4-
Jun	1									$(6)^{PT}$	5	2	6^{SZ}
Jul	1									$-2-^{PT}$	-4-		$(2)^{SZ}$
Aug	1									2	6		
Sep	2	1				(7)	3			5		6	
Oct	5	3			1^{NP}	6	2			4		1^{NA}	
Nov	3		1	9	10	-2-	8	6					
Dec	1	6	-2-	9^{EU1*}	4	8^{TNH*}	7	3				5	

* December EU1 and TNH are mixed *and* separated into modes 8 and 9. The stronger representation respectively is tabulated.

subsections 3a1–4, and the introductory material for sections 3b and 3c. These contain additional material that supports the main themes discussed earlier and in the conclusion, so they should be read in turn.

a. One month winter patterns[3]

1) NORTH ATLANTIC OSCILLATION (NAO)

The North Atlantic Oscillation (NAO; Fig. 2) is the only pattern found unambiguously in all 12 months, although it exhibits pronounced seasonal variation in its location. It contains a strong center over or just west of Greenland with a strong north–south gradient to the south having large zonal extent. Centers of opposite sign are found over the Atlantic, Europe or the United States, or all three or two out of three, or an elongated band over those zones may appear. In winter, the Greenland center is near 70°N, 40°–60°W with zero line near 50°N (Figs. 2l, 2a–b) and the Atlantic center is at 30°–35°N. A somewhat weaker center of sign like that of the Atlantic center is found in eastern Asia at 40°–50°N, 120°–140°E. In summer, the Greenland center is near 70°–75°N with zero line 50°–60°N, the Atlantic center is as far north as 40°–50°N, and a southern zero line near 30°–35°N appears (Fig. 2f–h). The eastern Asian center is weak or absent during the warm half of the year. The NAO's seasonal north–south contraction/expansion parallels that of the other basic meteorological features in the hemisphere (the profile of the westerlies, the 700 mb isotherms, etc.) in response to the annual cycle in solar insolation.

The RPCA loading patterns for the NAO have more month-to-month similarity from July to January (Figs. 2g–l, 2a, respectively) than from January to July (Figs. 2a–g, respectively). The latter highlight two patterns that deviate somewhat from those in adjacent months, namely the patterns for February (Fig. 2b) and April (Fig. 2d). In February, the NAO actually manifests itself on two modes, the stronger of which is shown in the figure. Note that the central Atlantic center is weak and subordinate to the European center. This mode also contains the EU2 pattern, to be described in section 3a7. The second, weaker mode and the composite of the two modes are discussed in more detail and shown in section 4c.

Even more striking are the differences between the April pattern and similar March and May NAO patterns (Figs. 2c and 2e). One clue to these differences is the relatively weak NAO mode number listed for April in Table 2. If the typical lifetimes of NAO events are shortest in April (i.e., the mode is most unstable), then the mode will be affected by the 30-day mean filter more in this month than in adjacent months. For example, the result of applying a 30-day mean filter to waves with periods of less than 30 days will be damping and distortion (see Fig. 15 in Panofsky and Brier, 1968), both of which seem to be the case here. This idea was suggested by the 10-day mean RPCA in which a prototypical NAO was obtained as the first mode for April (to be presented in section 3d), in sharp contrast to the 30-day mean result discussed above. In other words, in the case of a higher-frequency cutoff filter, much of the damping and distortion was alleviated.

It should be noted that although relative weaknesses in explained variance and mode number are also indicated for the NAO in October in Tables 1 and 2 respectively, several differences remain between October and April: The October NAO pattern (Fig. 2j) is more like the prototype and has comparable mode number in 30-day and 10-day mean analyses (5 vs 4), and adjacent months also have mode numbers greater than one. Thus, either the NAO behaves differently in the fall than it does in the spring, or the sampling dif-

[3] Standardized principal components (time series) for the major wintertime patterns described in subsections 3a1–4 for selected months are tabulated in appendix F as supplementary information.

Unauthenticated | Downloaded 08/21/22 12:56 PM UTC

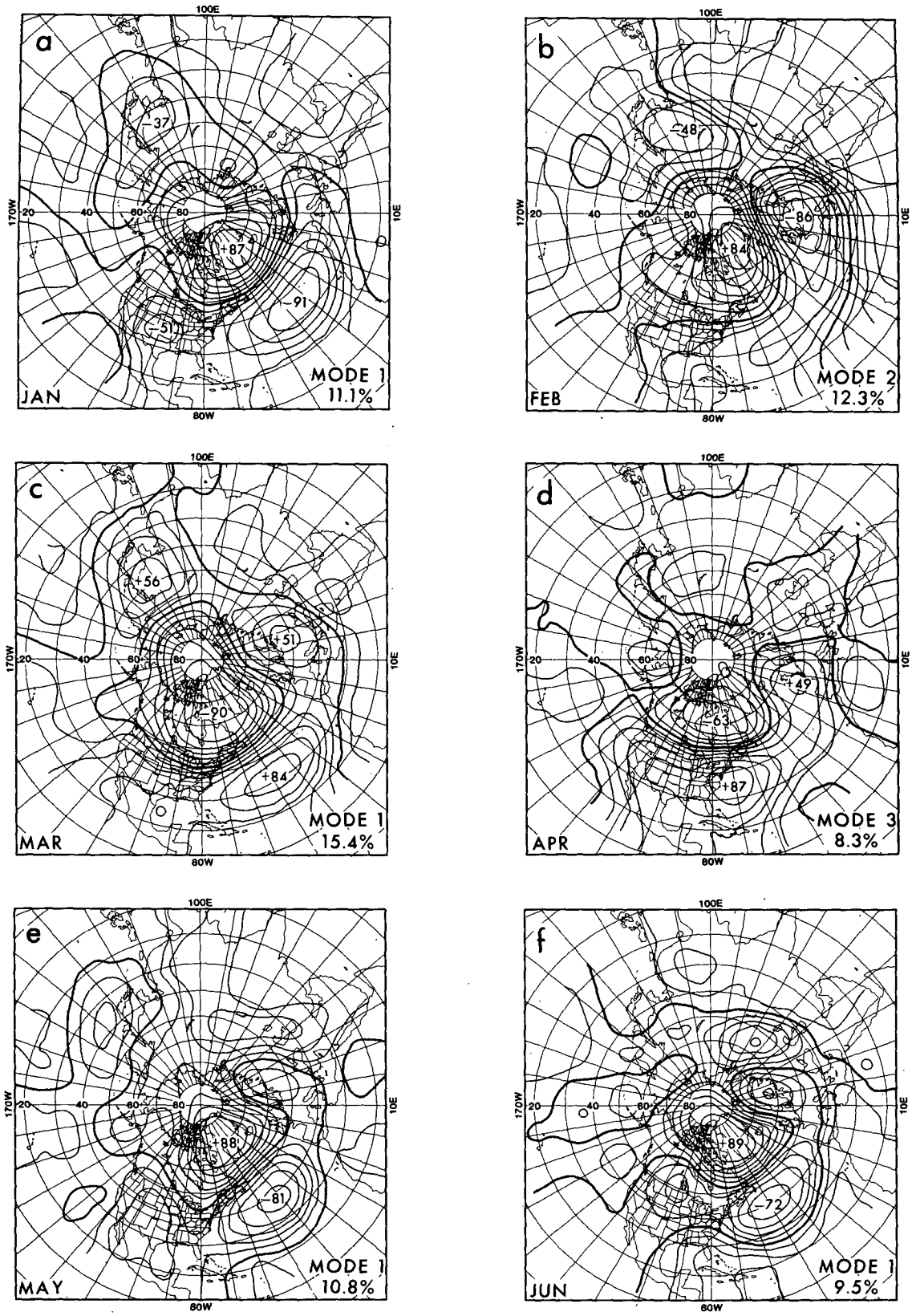

FIG. 2. The North Atlantic Oscillation (NAO) in (a) January (mode 1; prototype), (b) February (mode 2), (c) March (mode 1), (d) April (mode 3), (e) May (mode 1), (f) June (mode 1).

Unauthenticated | Downloaded 08/21/22 12:56 PM UTC

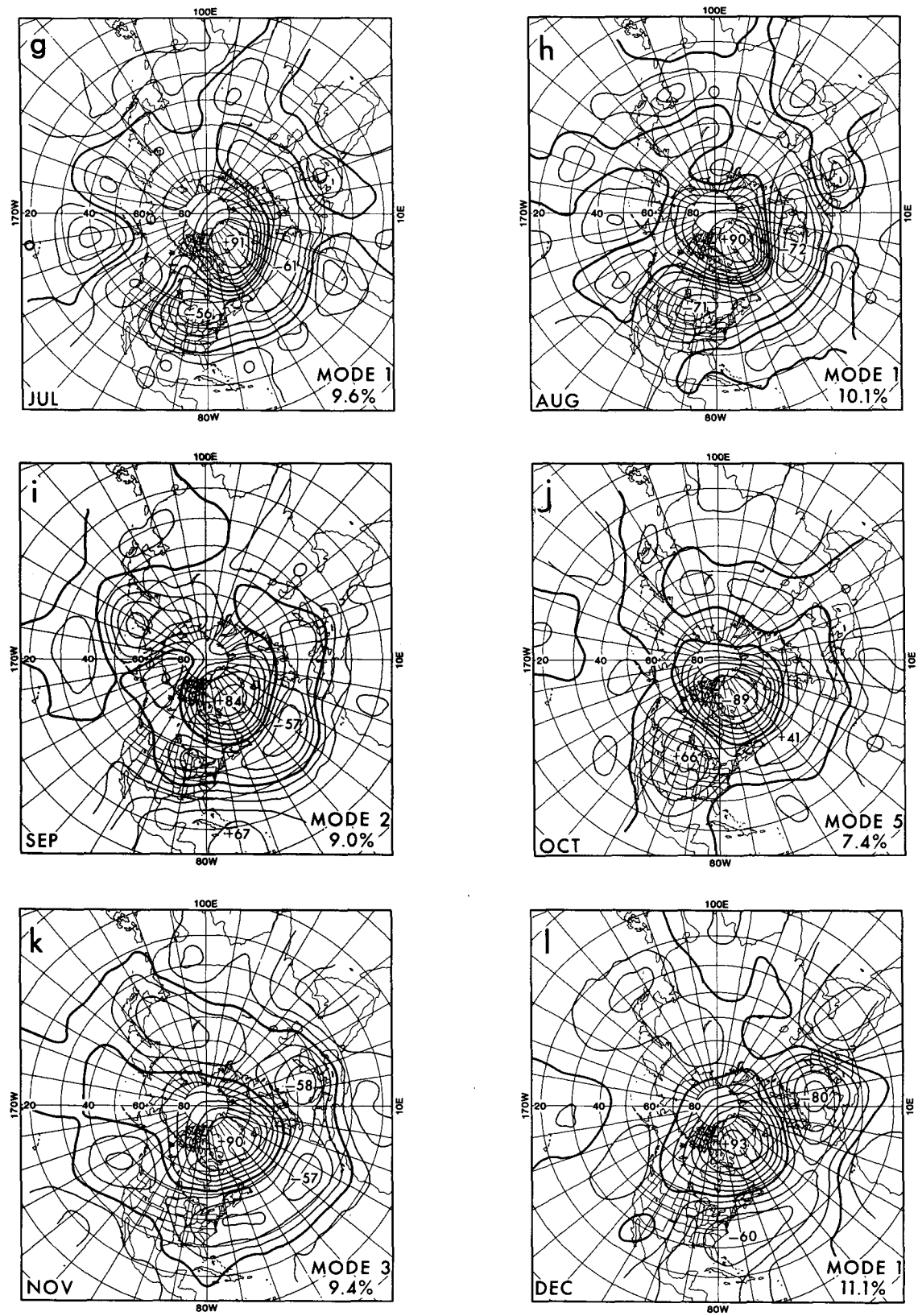

FIG. 2. (*Continued*) (g) July (mode 1), (h) August (mode 1), (i) September (mode 2), (j) October (mode 5), (k) November (mode 3), (l) December (mode 1). Contour interval is 0.15.

Unauthenticated | Downloaded 08/21/22 12:56 PM UTC

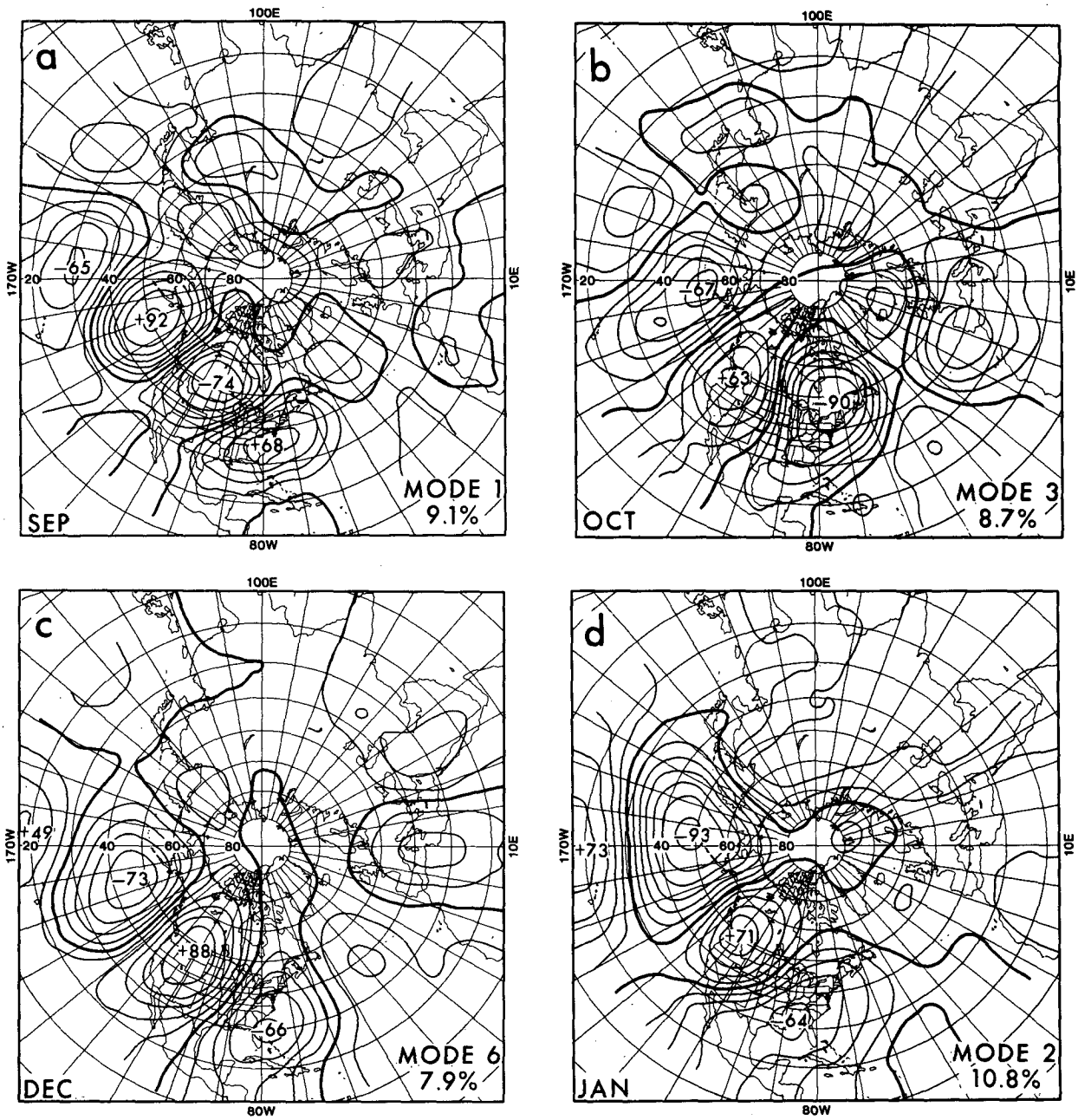

FIGURE 3

ficulties hypothesized for April were fortuitously avoided in October. Further analysis will be required to resolve this question.

Our study's January NAO is found in all five of the comparative winter studies. It corresponds to the 700 mb intermonthly as well as interannual teleconnection signals of the Western Atlantic and Zonally Symmetric Seesaw in E. The WG West Atlantic 500 mb teleconnection pattern is the closest match in that analysis to our NAO. For the 15-year RPCA results in H81, the best correspondence is with mode 5, although it is somewhat westward-displaced, while in H81's 30-year analysis mode 10 corresponds reasonably well to our NAO. In HW, the Atlantic Pattern (the 500 mb pattern associated with mode 1 of the RPCA of sea level pressure) matches our NAO, and in the obliquely rotated RPCA of 700 mb heights in LT, the January mode 2 is the NAO. Thus, the NAO is clearly recognizable in winter studies using either of the two general analysis methods for several levels of the atmosphere. Because it is active all year and appears as the leading or second mode in 9 out of 12 months, it easily ranks as the strongest contributor to low-frequency height variance in the Northern Hemisphere.

Unauthenticated | Downloaded 08/21/22 12:56 PM UTC

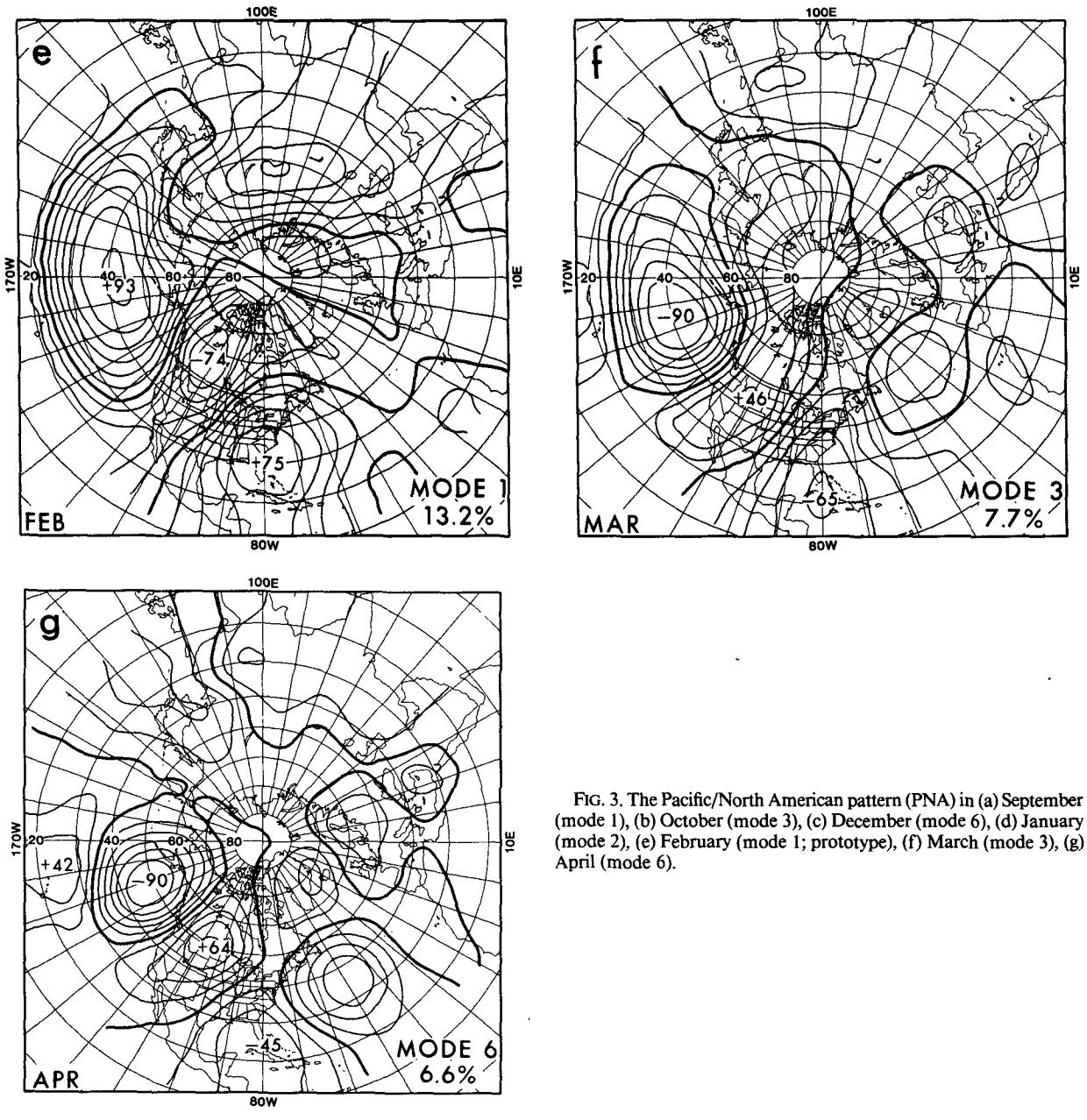

FIG. 3. The Pacific/North American pattern (PNA) in (a) September (mode 1), (b) October (mode 3), (c) December (mode 6), (d) January (mode 2), (e) February (mode 1; prototype), (f) March (mode 3), (g) April (mode 6).

2) PACIFIC/NORTH AMERICAN PATTERN (PNA)

In the cold season Pacific/North American pattern (PNA; Fig. 3), a strong center south of the Aleutian Islands at 40°–50°N is near 170°W in midwinter, otherwise 150°–160°W. A center of opposite sign is near 50°N (but may be north–south-elongated), 105°–125°W, near the United States–Canadian border between the Pacific Ocean and Rocky Mountains. A center of sign like that of the Aleutian center is near the southeastern United States—more toward Cuba in spring, more over the U.S. middle Atlantic coast in fall. A fourth center of sign opposite that of the Aleutian center appears to its south near 20°–30°N, 170°W (at the edge of the analysis domain). Figure 3 illustrates the symmetry of the seasonal progression of the PNA pattern, in which it begins in December (Fig. 3c) and ends in April (Fig. 3g) with only moderate strength (mode 6), a relatively short wavelength and a Pacific center of only moderate size. The lengthening then shortening of the wavelength is reminiscent of the wavelength dependence of Rossby-like wavetrains on the seasonal strengthening and weakening of the extratropical westerlies. In February, the PNA attains

Unauthenticated | Downloaded 08/21/22 12:56 PM UTC

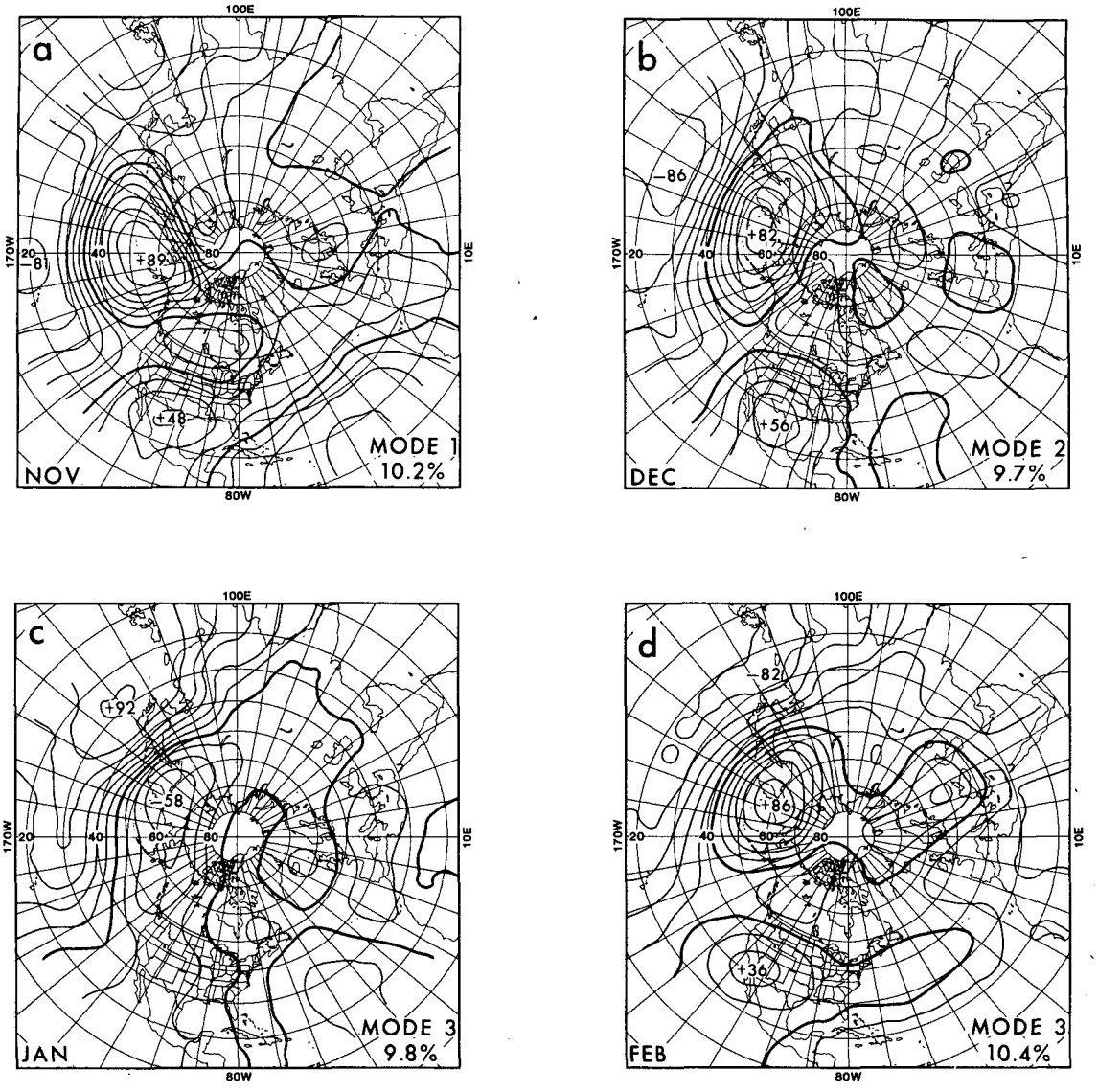

FIGURE 4

maximum strength (mode 1), and has maximum wavelength and a giant Pacific center. The September–October appearances of PNA (Figs. 3a, b) are consistent with the December–April progression in terms of wavelength but not strength, and are separated by a November absence (see subsection 3a3 for a possible explanation).

The PNA is replicated with greater fidelity in the five other studies than any other pattern; perhaps this is why it is always referred to by the same name. It appears in fine form in the interannual and intermonthly signals in E, in WG, in H81 (mode 2 in the 15-year analysis, mode 1 in the 30-year analysis), in HW (mode 6) and in LT (mode 4).

3) WEST PACIFIC OSCILLATION (WPO)

The cold season West Pacific Oscillation (WPO; Fig. 4) has a strong center over or somewhat east of Kamchatka at 50°–60°N, 160°E–170°W, a zero line at 35°–45°N and an oppositely signed east–west Pacific anomaly band at 20°–30°N, 160°W–130°E. The south and central United States often has a moderately strong center with sign like that of the Kamchatka center. The WPO tends to be found progressively westward from fall to winter, and then in more easterly positions in spring (May is the only exception). In March and April (Figs. 4e, f), the WPO modes are mixed with the warm season SZ pattern, to be defined in subsection 3b2.

Unauthenticated | Downloaded 08/21/22 12:56 PM UTC

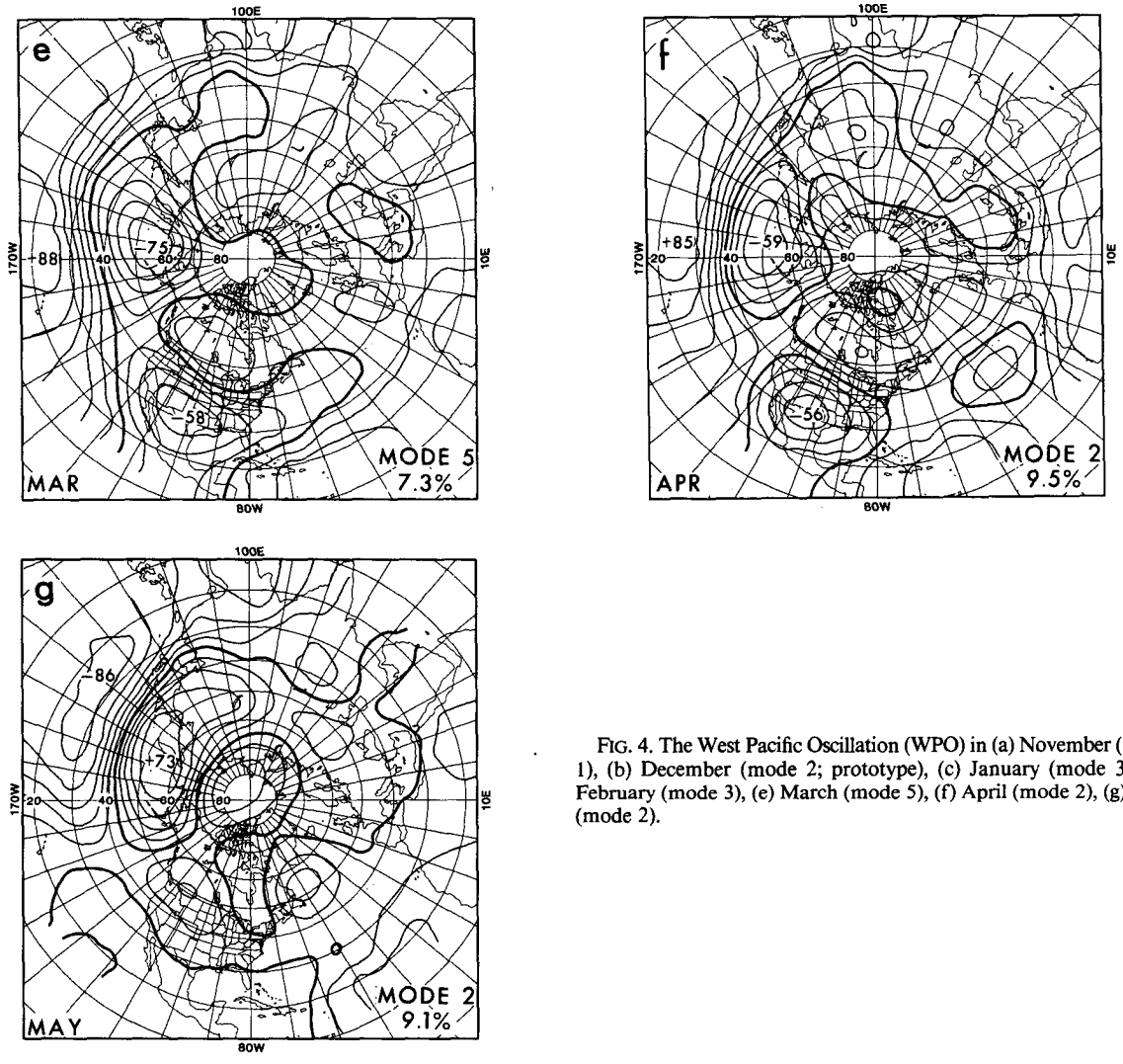

FIG. 4. The West Pacific Oscillation (WPO) in (a) November (mode 1), (b) December (mode 2; prototype), (c) January (mode 3), (d) February (mode 3), (e) March (mode 5), (f) April (mode 2), (g) May (mode 2).

The WPO appears in all five other studies. It is called the Western Pacific pattern in E, featuring a less prominent United States center. It corresponds well to the WG Western Pacific pattern, the mode 1 pattern in H81's 15-year study and the mode 3 pattern in his 30-year study, and the mode 1 pattern in LT. In HW, it is found in the Pacific pattern except with an eastward translation similar to the November version of WPO in the present study, in which it may have absorbed the weak remnant of a missing PNA pattern.

4) TROPICAL/NORTHERN HEMISPHERE PATTERN (TNH)

The Tropical/Northern Hemisphere pattern (TNH; Fig. 5), whose North American features are shifted eastward with respect to those of a PNA pattern so as to be out of phase with it, has a center just off the Pacific northwest coast of the United States at 40°–50°N, 125°–140°W, an oppositely signed center near or just north of the U.S. Great Lakes at 45°–55°N, 80°–90°W, and a broad center of sign like that of the Pacific center near or just east of Cuba. A somewhat weaker center with the same sign as that of the oceanic centers appears during the three winter months in eastern Asia at 35°–50°N, 105°–115°E. This, along with its unambiguous linkage to the tropics by Mo and Livezey (1986), has led us (K. C. Mo and the present authors) to designate the pattern as TNH. Mo and Livezey (1986) found the pattern through teleconnection statistics from tropical station geopotential heights. Note from Table 2 that the December TNH is mixed with EU1 (defined in subsection 3a6) and that both are apparently separated onto two December modes (Figs. 5b and 7c). The more representative mode is displayed for each pattern, respectively.

Although classified for the first time in Mo and Livezey (1986), the TNH has appeared in one form or an-

Unauthenticated | Downloaded 08/21/22 12:56 PM UTC

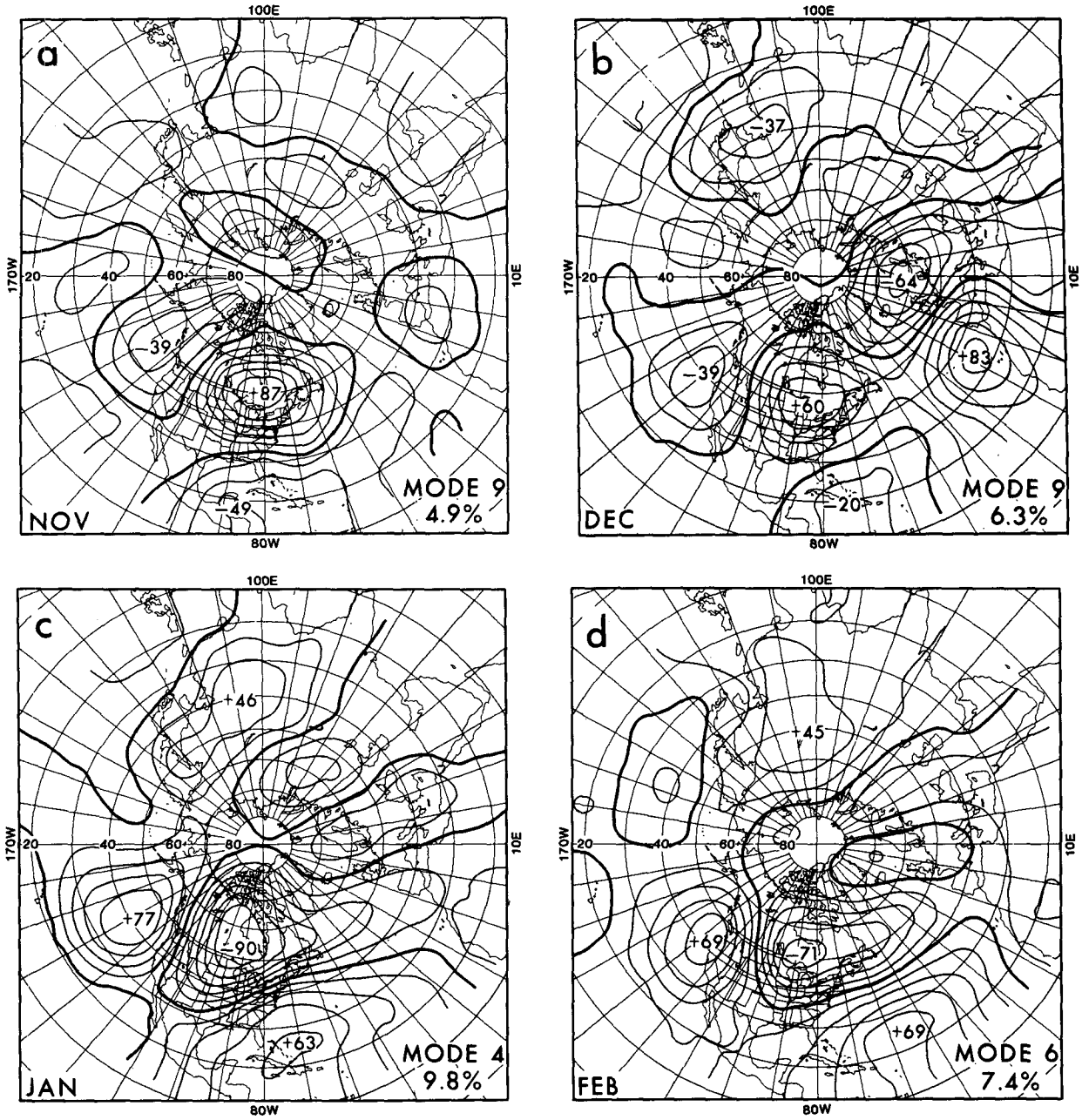

FIG. 5. The Tropical/Northern Hemisphere pattern (TNH) in (a) November (mode 9), (b) December (mode 9), (c) January (mode 4; prototype), (d) February (mode 6).

other in four of the five comparative studies. The interannual signal of the Zonally Symmetric Seesaw in E, although most strongly suggestive of NAO, clearly contains TNH and EU2 (to be described shortly) elements as well, depending on the base point location. WG does not classify the TNH, but their summary of strongest negative correlations for each grid point in their one-point correlation analyses (see their Fig. 7b) shows a small relative maximum area between Hudson Bay and the U.S. Great Lakes with $|r| > 0.6$. Although this value is surpassed by many of the other maxima in the hemisphere and was thus ignored, it is a base point from which a TNH teleconnection pattern would have been produced, as will be shown in section 4c. The 15-year analysis in H81 paints a crude picture of the TNH with mode 6, which supplies the Pacific center and the Canadian center. The southern center of mode 5 may be a mixture of the Atlantic centers of both the TNH and NAO. Mode 5 of the 30-year analysis in H81 quite closely corresponds to the TNH. In H81's discussion the Pacific center was not mentioned and the two eastern centers were likened to the WG Western

Unauthenticated | Downloaded 08/21/22 12:56 PM UTC

Atlantic pattern. The TNH appears in good form in mode 7 in LT.

5) NORTHERN ASIAN PATTERN (NA)

The Northern Asian pattern (NA; Fig. 6) features a strong anomaly center over or near the Taymyr Peninsula at 70°–80°N, 70°–130°E and a weaker, oppositely signed center over Mongolia at 45°–50°N, 100°–120°E in all months except December and January, during which it appears in the central or western Pacific at 30°–40°N, 165°–180°E. In October (Fig. 6a) the NA is mixed with the NP pattern (subsection 3c1), and in March (Fig. 6f) with EU1 (subsection 3a6). The NA is found in four of the five other studies: in the intermonthly signal of the Northern Asian pattern in E, in mode 4 of the 15-year analysis of H81, as the Siberian Pattern (mode 2) in HW and with an additional European center in mode 5 of LT.

6) EURASIAN PATTERN TYPE 1 (EU1)

The Eurasian pattern Type 1 (EU1; Fig. 7) has a vigorous center at 60°–70°N, 25°–50°E, an oppositely signed somewhat weaker center in northwest China or western Mongolia (southwest of Lake Baykal at 30°–45°N, 80°–100°E), and, except for well into the spring, an area in Spain and the adjacent Mediterranean and Atlantic (35°–50°N, 10°E–20°W) of sign opposite that of the Scandanavian center. A fourth center in this roughly east–west sequence often appears weakly over Japan (30°–40°N, 130°–140°E) as well. The March version is mixed with NA (Fig. 6f), and the December version (Fig. 7c) is separated and mixed with TNH (Fig. 5b).

The EU1 pattern emerges in all five other studies but not in a straightforward manner in all cases. In E, it unquestionably appears in both intermonthly and interannual signals of the Eurasian pattern, having the Japanese center and not the Spanish center. The Japanese center version of EU1 also is found to be well represented in WG in the Eurasian pattern. The H81 15-year analysis provides the Asian and Japanese centers of EU in mode 8 and the Scandanavian center in mode 10, again without a center over Spain. The pattern appears with all four centers in proper phase in LT's mode 10. In HW, the Chinese Pattern (mode 4) captures only the Japanese and Mongolian centers, making for a partial pattern correspondence.

7) EURASIAN PATTERN TYPE 2 (EU2)

The Eurasian pattern Type 2 (EU2; Fig. 8) is a 3-center east–west pattern with western center near England or Denmark at 50°–60°N, 10°W–10°E, an oppositely signed center near or just north or northeast of the Caspian Sea at 40°–50°N, 50°–60°E, and a center with sign like that of the British center in northeast China (just north of Korea) at 40°–50°N, 115°–135°E. The EU2 pattern bears some structural similarity to EU1, the most important difference being the east–west phase shift, rendering the two patterns essentially orthogonal. The October (Fig. 8a) and December (Fig. 8c) patterns have a relatively weak Chinese center (especially December) and an additional upstream center in the Atlantic. The February pattern is mixed with NAO (*Fig. 2b*).

The EU2 pattern occurs on a weaker mode in January than the EU1, and is found only in three out of five of the comparative studies. The intermonthly and interannual signals of the Eastern Atlantic pattern in E contain both our EA (to be described below) and EU2 patterns; in the latter case, the British center is displaced somewhat northwestward, but the other centers correspond well to ours. Esbensen's interannual signal of the "zonally-symmetric seesaw," in addition to containing our NAO to a large extent, has suggestions of TNH and EU2. Mode 9 in the 15-year analysis in H81 corresponds to our EU2, as does mode 9 in LT.

8) EAST ATLANTIC PATTERN (EA)

The East Atlantic pattern (EA; Fig. 9) is defined by a center near 55°N, 20°–35°W with a strong northwest–southeast gradient over western Europe (zero line always through England or France) and an oppositely signed east-northeast–west-southwest-oriented anomaly band over North Africa or the Mediterranean Sea with most likely location 25°–35°N, 0°–10°W. The EA pattern is represented in all five other studies but not always in pure form. It is found in the intermonthly signal of E's Eastern Atlantic pattern, although the northern Atlantic center is shifted eastward such that a blend of EA and EU2 is created. The WG Eastern Atlantic pattern is an approximate match, except that it has a more prominent Black Sea center than does our EA. In H81, mode 2 in the 30-year analysis is a better match than mode 3 in the 15-year analysis because it is situated farther east. The HW study apparently produced an EA (mode 5) which was not named or illustrated, but was described as a "north–south seesaw with its major center over North Africa." The EA emerged in the LT study as mode 6.

9) EAST PACIFIC PATTERN (EP)

In the East Pacific pattern (EP; Fig. 10), the final cold season pattern in our inventory, a strong center near eastern Alaska (60°–65°N, 135°–150°W) is bounded by a high gradient to the south, a nearly east–west zero line near 40°–45°N and an oppositely signed center (possibly an east–west-oriented band) at 25°–30°N, 125°–140°W. The EP, though the weakest mode in our 1-month January analysis, is still represented in three out of the five comparable studies. It appears in the interannual signal of the North Pacific pattern in E, in mode 7 of the 15-year analysis in H81, and in mode 8 of LT.

Unauthenticated | Downloaded 08/21/22 12:56 PM UTC

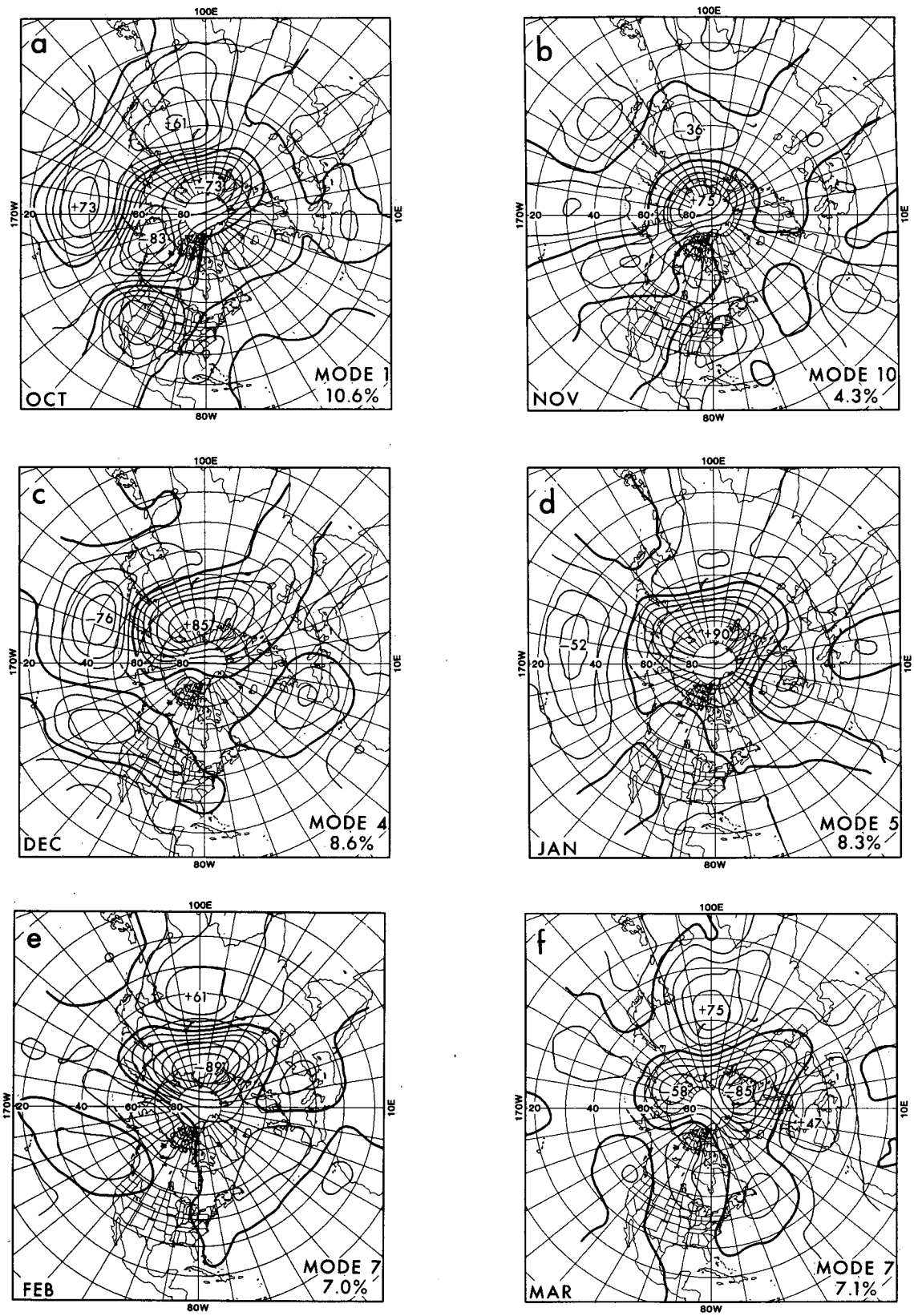

FIG. 6. The Northern Asian pattern (NA) in (a) October (mode 1), (b) November (mode 10), (c) December (mode 4), (d) January (mode 5; prototype), (e) February (mode 7), (f) March (mode 7).

Unauthenticated | Downloaded 08/21/22 12:56 PM UTC

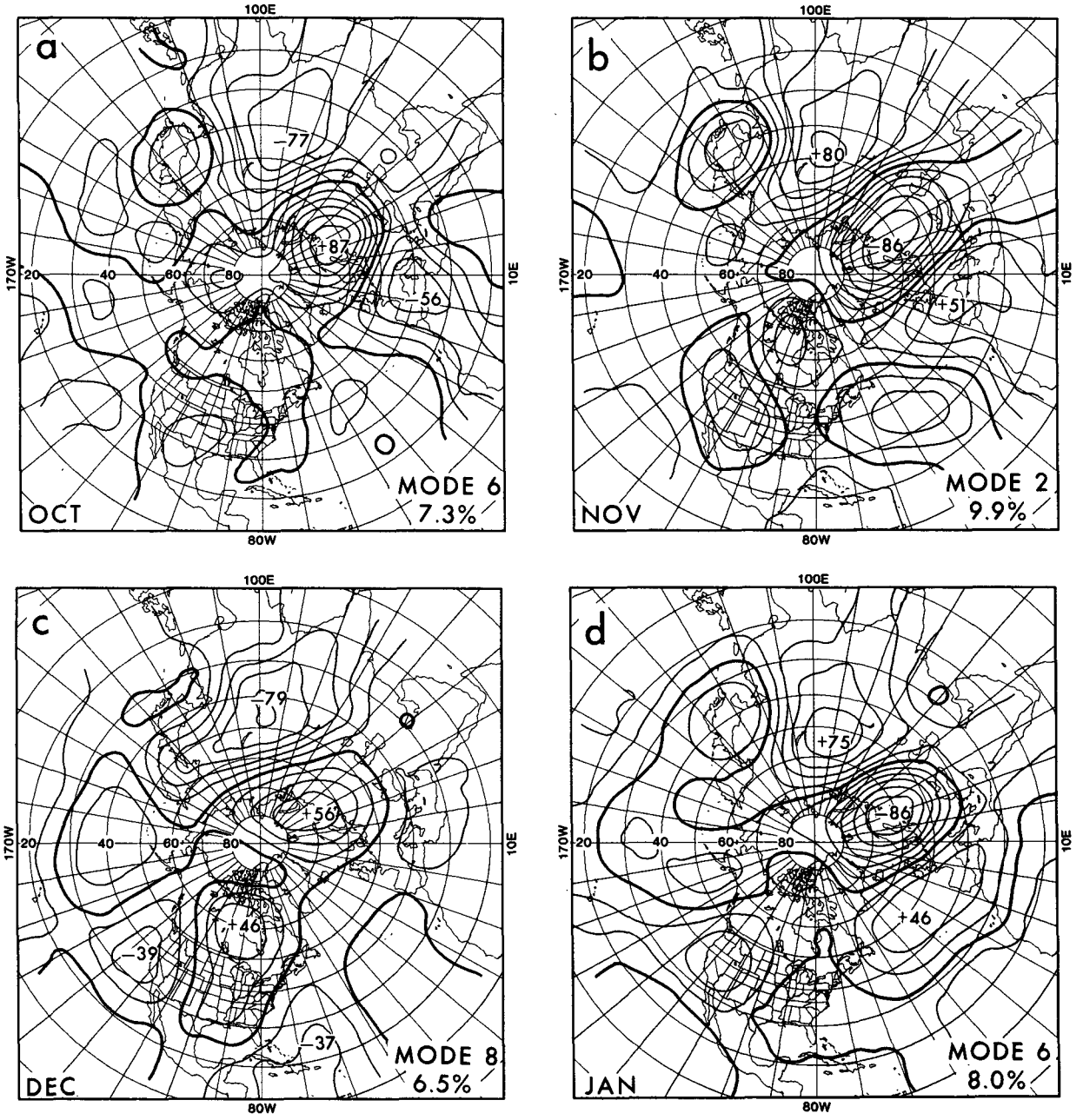

FIG. 7. The Eurasian pattern, type 1 (EU1) in (a) October (mode 6), (b) November (mode 2; prototype), (c) December (mode 8), (d) January (mode 6).

b. One-month summer patterns

Only the 30-year RPCA analysis in H81 and the obliquely rotated RPCA study in LT examine the summer circulation, which reduces the number of possible comparisons with our results. The table in appendix C summarizes the correspondences between their patterns and ours. Only two exclusively warm season patterns appear in our study (SZ and AS); the third (NAO) is an all-season pattern and a possible fourth (PT) is more of a spring/summer pattern that appears to become associated with SZ as its active period culminates in June and July.

1) NORTH ATLANTIC OSCILLATION (NAO)

The summer NAO (Figs. 2f–i) appears in mode 5 in H81 and mode 4 in LT, leaving no doubt about its reality in the warm season. In both other studies, it contracts northward with respect to the winter position, in agreement with our finding. In H81, it is shifted eastward as well with respect to its winter location,

Unauthenticated | Downloaded 08/21/22 12:56 PM UTC

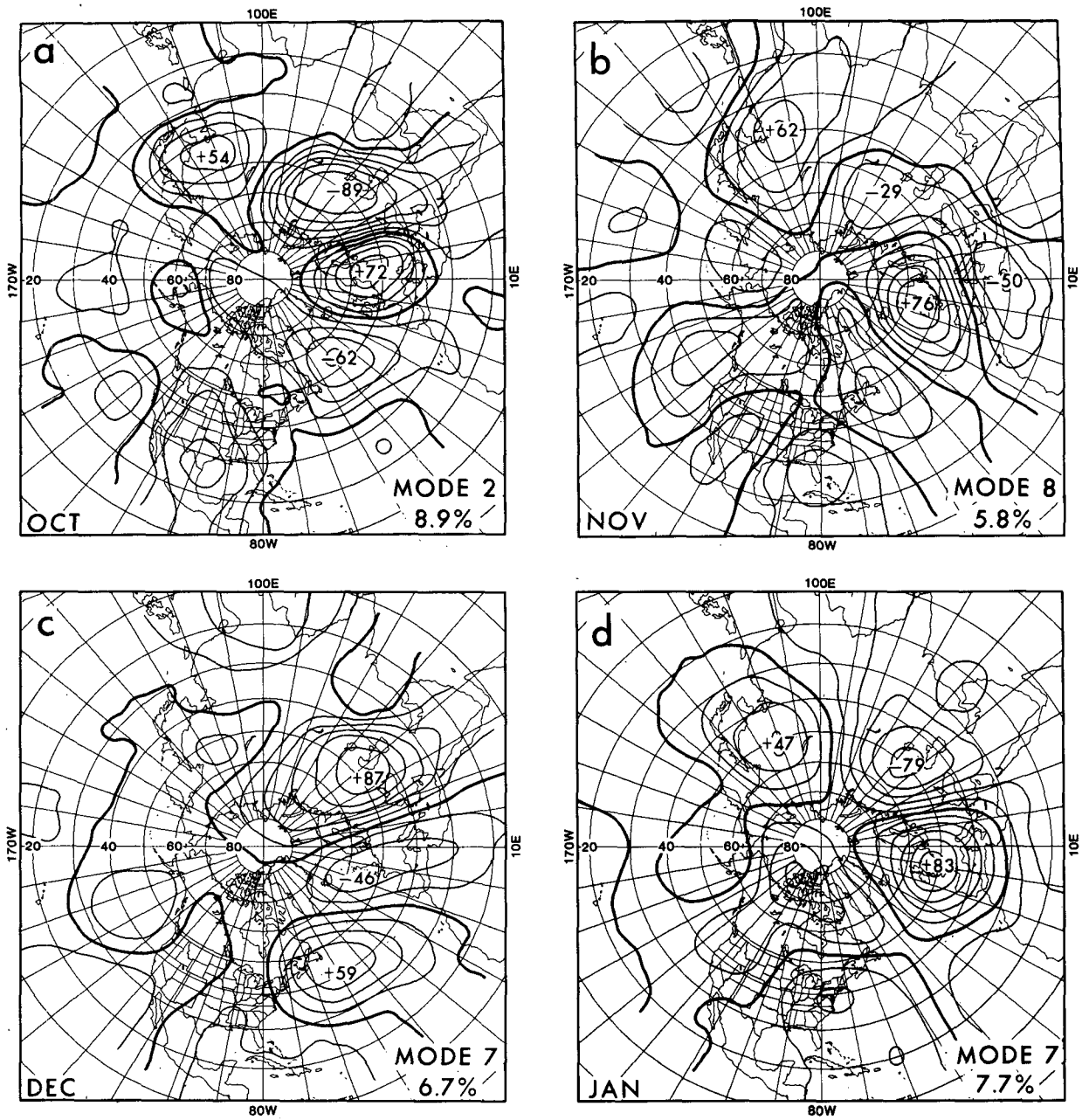

FIG. 8. The Eurasian pattern, type 2 (EU2) in (a) October (mode 2), (b) November (mode 8), (c) December (mode 7), (d) January (mode 7; prototype).

coinciding more closely with our NAO longitude at all times of the year.

2) SUBTROPICAL ZONAL PATTERN (SZ)

In the warm season Subtropical Zonal (SZ; Fig. 11) pattern, an east–west band of like-signed loadings appears south of 30°–35°N in three preferred regions: 1) the Pacific, 2) the Caribbean and west Atlantic, and 3) North Africa. The SZ pattern is an index of zonal flow conditions at 25°–35°N; it is the only pattern having quasi-hemispheric longitudinal extent. In the spring, the SZ is associated with the WPO pattern (Figs. 4e–f), and in June (Fig. 14c) and July (Fig. 11a) it appears together with the PT pattern (subsection 3c2). The SZ appears strongly in both other summer studies, but is confounded by the subtropical data bias in the early and middle 1950s (see appendix A). In H81, the Pacific sector of SZ appears in mode 2 while mode 3 supplies the North African sector. Similarly, in LT mode 1 gives all but the Pacific sector, which is covered by the combined SZ and PT patterns of mode 3. The data bias tends to cause the SZ to appear on two modes, one of which contains most of the bias feature.

Unauthenticated | Downloaded 08/21/22 12:56 PM UTC

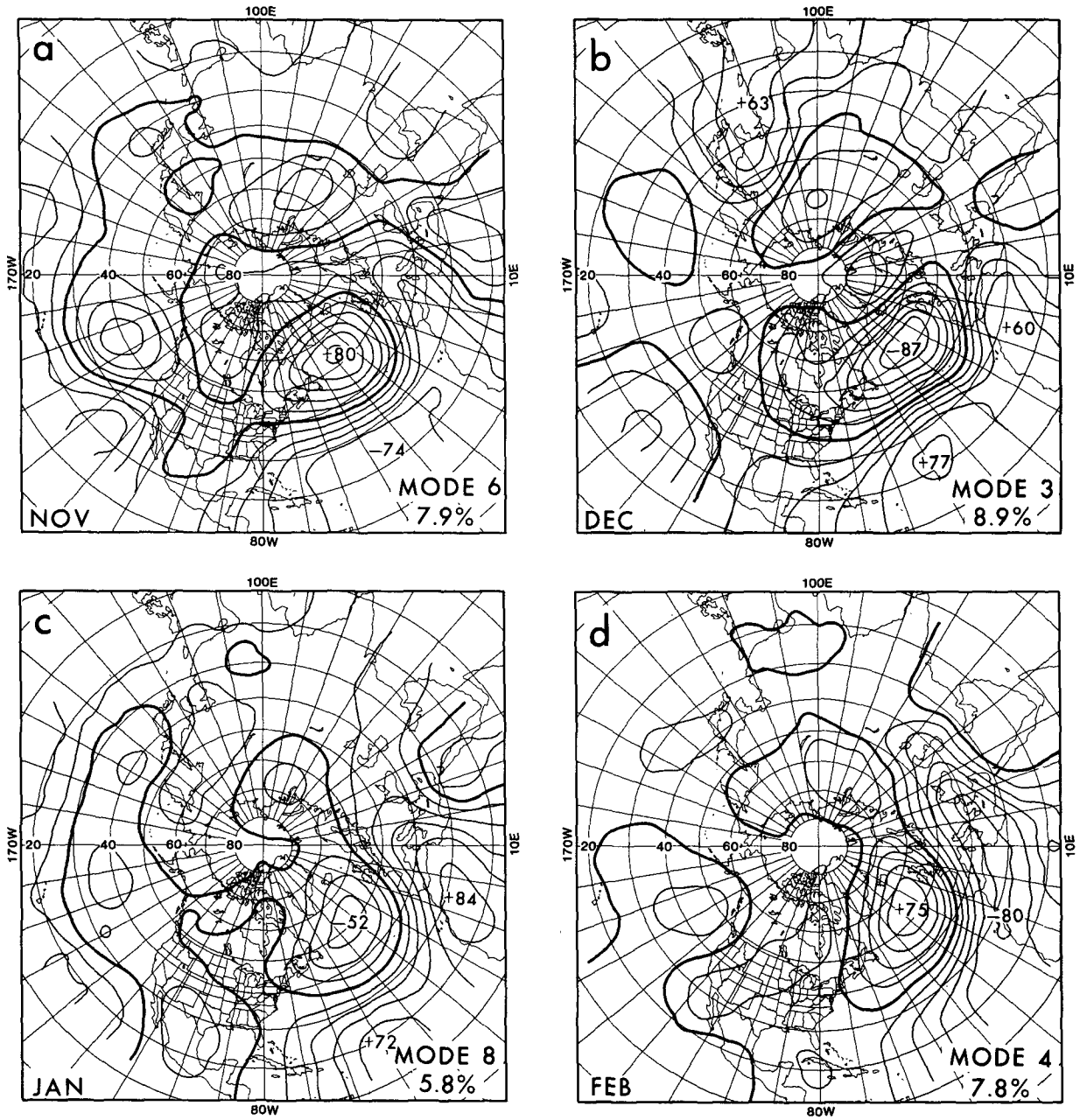

FIG. 9. The Eastern Atlantic pattern (EA) in (a) November (mode 6), (b) December (mode 3), (c) January (mode 8), (d) February (mode 4; prototype).

3) ASIAN SUMMER PATTERN (AS)

In the Asian Summer pattern (AS; Fig. 12), the strongest feature on the map is a broad, east–west center in central Asia at 40°–50°N, 40°–100°E. Loadings of opposite sign tend to reside to the north, including Novaya Zemlya and sometimes the pole. The AS appears in mode 7 in H81 and in mode 7 in LT.

Despite hopes of finding a stable North American summer heat-wave circulation pattern, only a marginally suggestive pattern was produced in July, August and September. Because this RPCA solution does not pass the robustness criteria to be described in section 4, the pattern is not classified. (RPCA of 1000–700 mb thickness does yield a more promising heat-wave-like pattern.)

c. One-month transition season patterns

Other than in the present study, the patterns of the transition seasons have only been examined in LT using the oblique rotation RPCA. In general, there is good correspondence between their results and ours, as shown in the tables in appendix D for April and Oc-

Unauthenticated | Downloaded 08/21/22 12:56 PM UTC

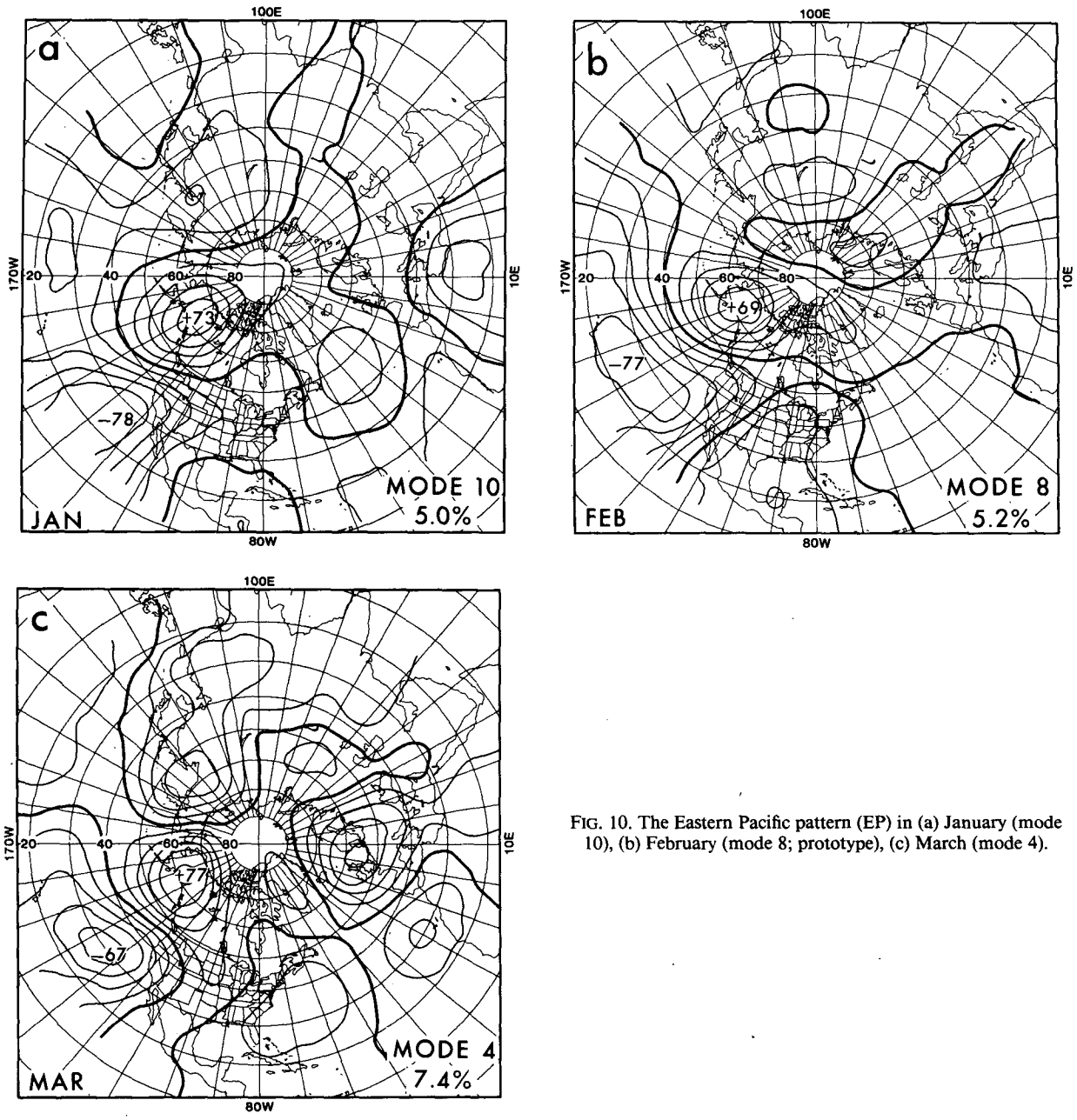

FIG. 10. The Eastern Pacific pattern (EP) in (a) January (mode 10), (b) February (mode 8; prototype), (c) March (mode 4).

tober. Some of the patterns described in appendix D are basically cold season patterns having long seasonal cycles that cover the transition months (PNA, EU1, EU2, EA and WPO), or likewise for warm season patterns (SZ) or all-season patterns (NAO). The NP (spring/fall) and PT (spring/summer) are the only two patterns with seasonalities centered in one or both of the transition seasons.

1) NORTH PACIFIC PATTERN (NP)

The North Pacific pattern (NP; Fig. 13) appears mostly in spring and fall, but also in December, and is defined by a peanut-shaped pair of like-signed mutually embedded centers, one in the central North Pacific at 35°–45°N, 160°–175°W (nearer to 35°N in winter, 45°N in summer) and the other near Korea at 30°–45°N, 120°–135°E. A strong gradient to the north of this dual center area (with zero line close to 60°N) leads to a center or east–west-elongated band of opposite sign near or north of Bering Strait, possibly extending from 100°E to 130°W at 60°–80°N. The NP appears to reflect the strength of the westerlies in the 50°–70°N zone in eastern Asia and across the Pacific. The October NP solution is combined with NA (Fig. 6a). In April, our NP corresponds to the LT mode 8 which is somewhat eastward-translated, and in October their mode 1 is a good match.

Unauthenticated | Downloaded 08/21/22 12:56 PM UTC

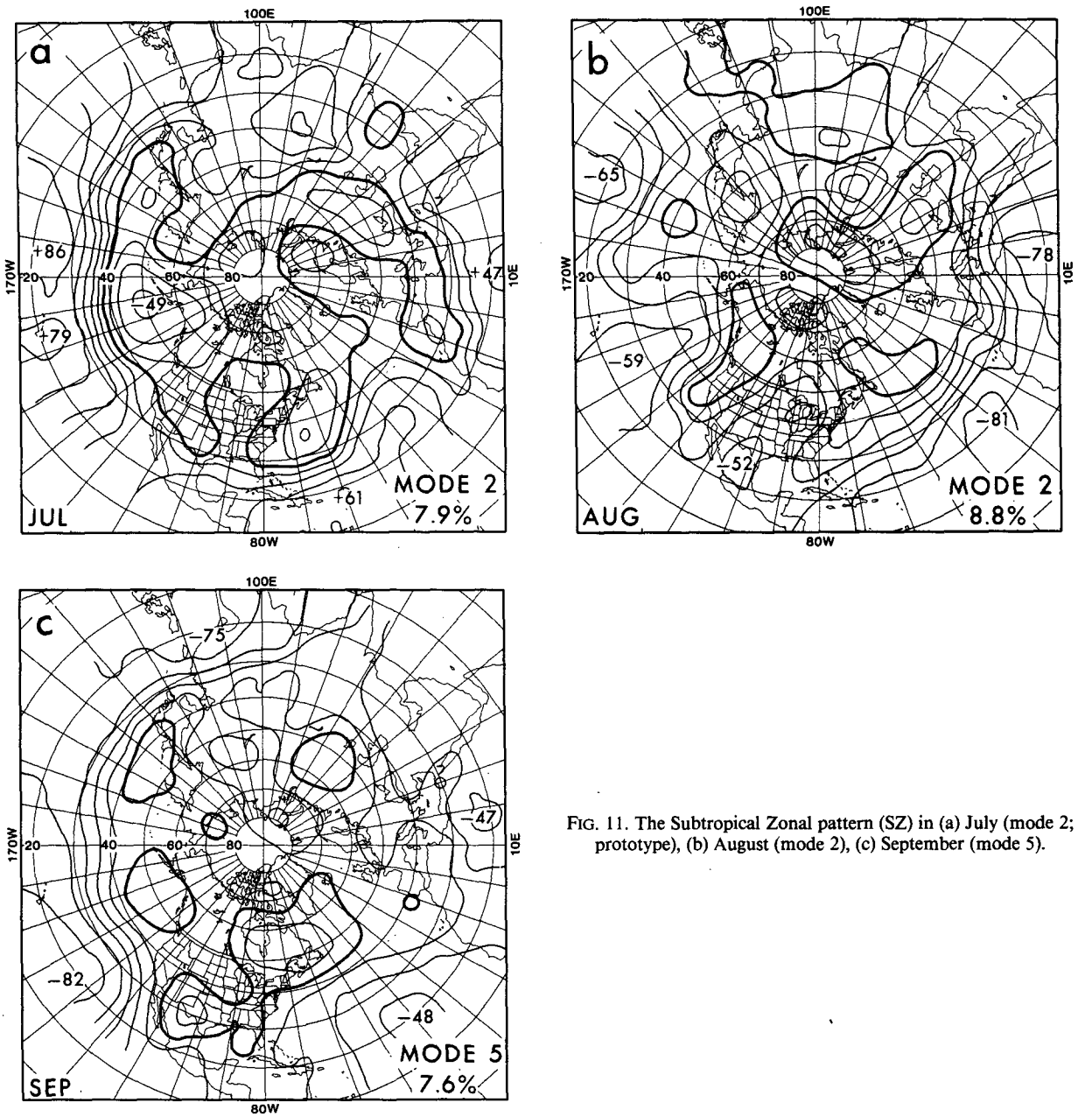

FIG. 11. The Subtropical Zonal pattern (SZ) in (a) July (mode 2; prototype), (b) August (mode 2), (c) September (mode 5).

2) PACIFIC TRANSITION PATTERN (PT)

The spring/summer Pacific Transition pattern (PT; Fig. 14), a pattern whose form and location show very strong seasonal dependence, has a broad east–west band of like-signed loadings in the subtropical Pacific, mostly south of 40°N and between 110°W and 140°E. A center of same sign is found in the eastern Soviet Union or Kamchatka (50°–60°N, 170°–120°E) with a typically weaker center of opposite sign in southwest Canada which may also include the west or central United States and northern Canada or the Arctic. The PT pattern centers appear successively further to the west between April and July, in that the northwesternmost center is gradually relocated from 60°N, 170°E in April (Fig. 14a) to 50°N, 140°E in June (Fig. 14c) to 50°N, 120°E in July (Fig. 11a), while the subtropical center occupies only the eastern Pacific in April, but the entire Pacific in July. These changes may be related to the weakening of the mean westerlies in spring. In June and July the PT appears together with SZ (Figs. 14c and 11a, respectively). The April PT appears shifted somewhat northwest in mode 5 in LT's April analysis, in which WPO and SZ are also found.

As appendix D indicates, most of our April and October patterns that are part of the seasonal cycles of warm or cold season patterns were also fairly faithfully replicated in the LT results.

Unauthenticated | Downloaded 08/21/22 12:56 PM UTC

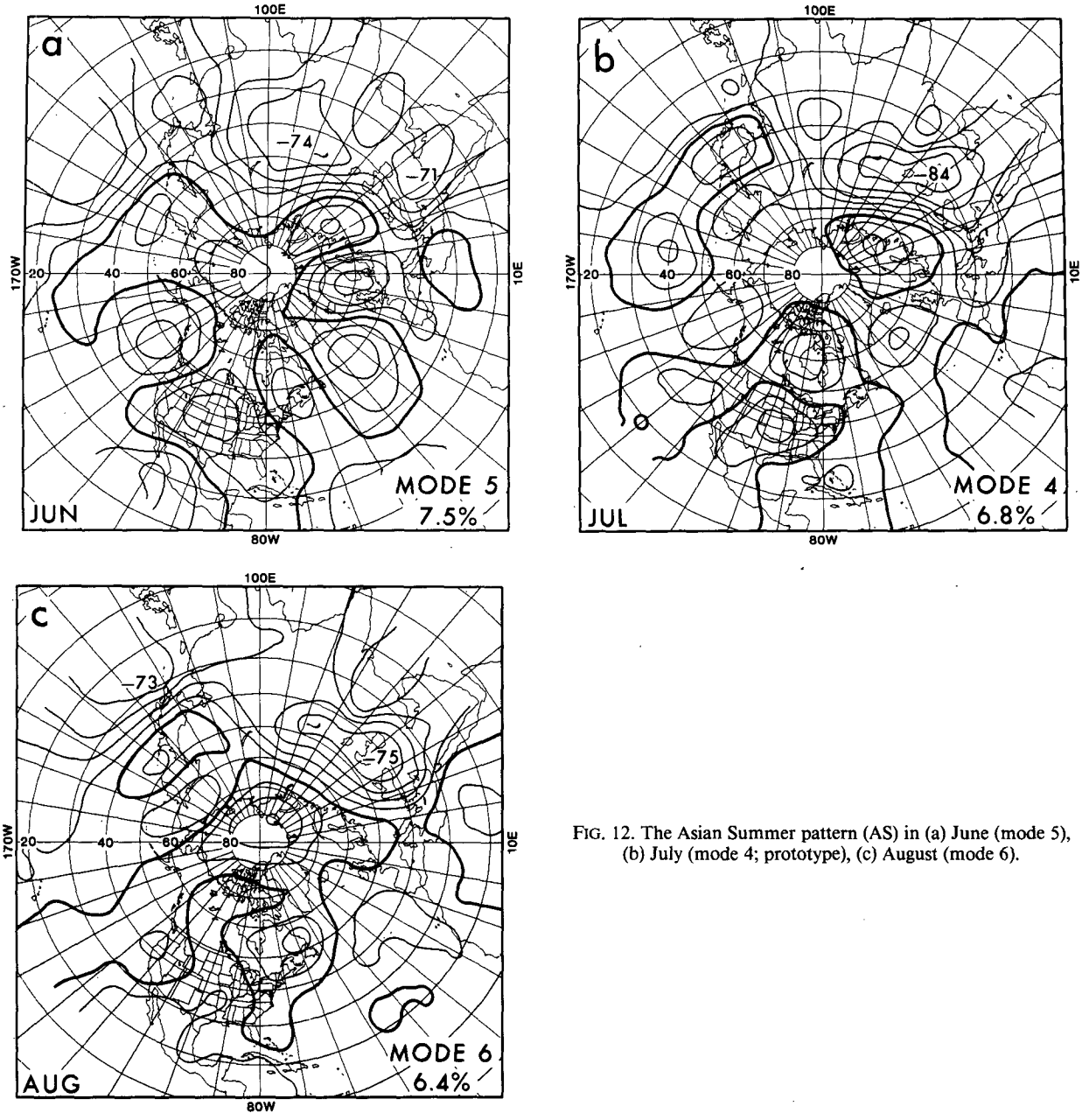

FIG. 12. The Asian Summer pattern (AS) in (a) June (mode 5), (b) July (mode 4; prototype), (c) August (mode 6).

d. Ten-day mean circulation patterns

As an additional comparative exercise relative to the 1-month results, 10-day mean 700 mb heights were analyzed, where 30 10-day means centered 1 day apart (i.e., 90% overlapping) were pooled for each month's RPCA. One would expect synoptic scale "noise" to play a greater role in 10-day than in 1-month results; the key question, however, is whether the low-frequency patterns still come through clearly. In the HW study, 5-day means of sea level pressure were used and five to six of the major low-frequency 500 mb patterns were still found in association with the leading modes of sea level pressure, suggesting that relatively short averaging periods constitute a good enough temporal filter to analyze most of the important quasi-stationary variability in the winter.

The 10-day results show strongly preserved low-frequency circulation patterns in all months. The only major difference from 1-month results is that the patterns of interest constitute a smaller portion of the total variance in the 10-day than in the 1-month solutions, reflecting the presence of a higher proportion of incoherent variability in the former. The first 10 modes for the 10-, 30-, and 90-day analyses for January (DJF for the 90-day) explain 67.5, 81.3, and 82.1 percent of the variance, respectively. The breakdown for summer

Unauthenticated | Downloaded 08/21/22 12:56 PM UTC

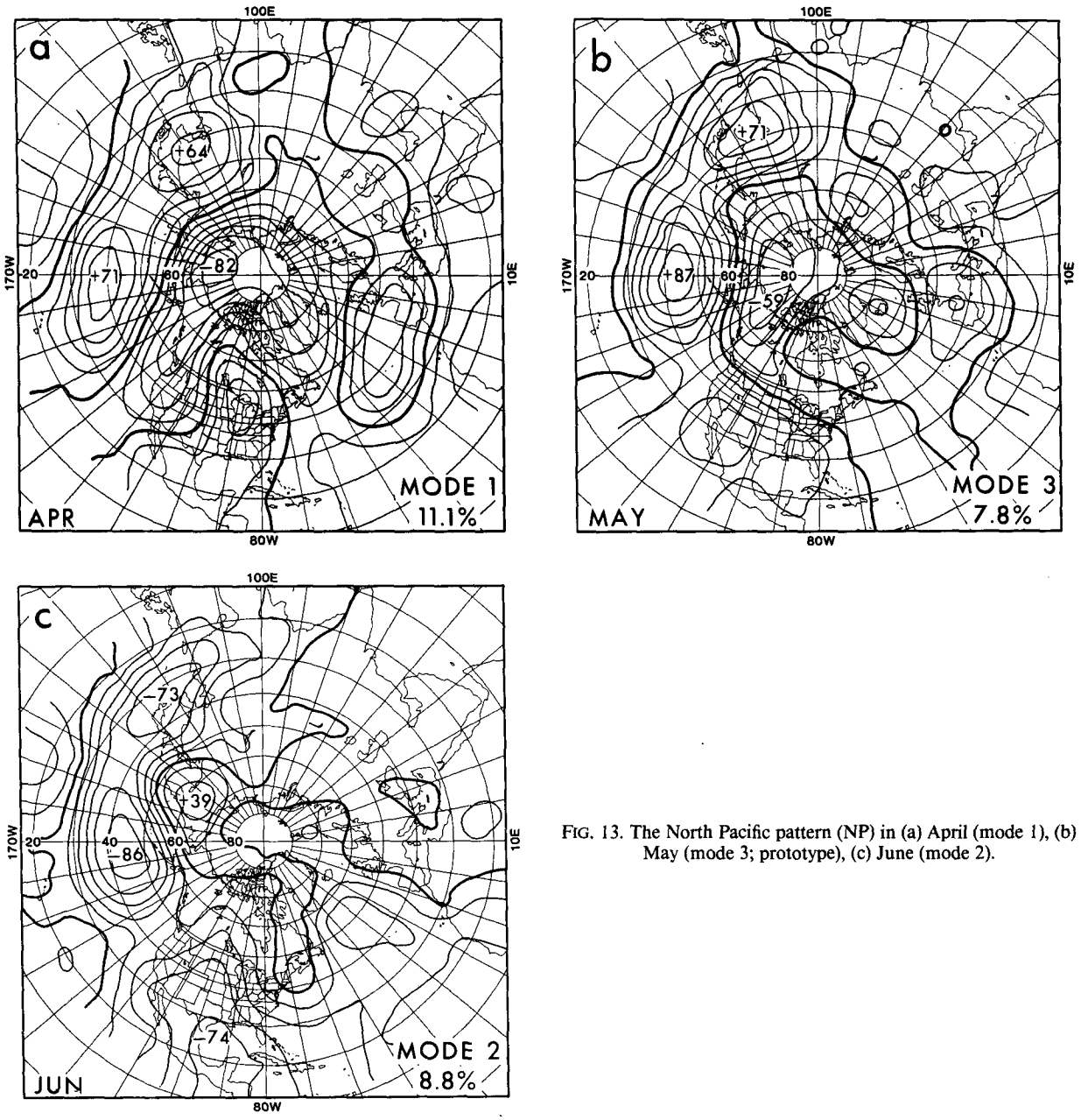

FIG. 13. The North Pacific pattern (NP) in (a) April (mode 1), (b) May (mode 3; prototype), (c) June (mode 2).

is comparable, except less variance is explained for all three of the averaging periods than for winter. Table 3 shows the correspondence between the 10-day and 1-month RPCA results for January, April, July and October, indicating the high degree of reproducibility of 1-month results using 10-day means. The April and October results probably would have had still greater correspondence with 1-month results if the annual cycle had been removed from the 10-day data. Because it was not, the march of the annual cycle appeared as one of the unmatched modes in April (mode 3) and October (mode 5), in which the sign of the slope of the principal component time series from the beginning to the end of the month was consistent from one year to another. (The associated loading patterns of the annual cycle modes were largely zonally symmetric with the polar region having opposite sign from the middle latitudes, the latter region reflecting the direction of seasonal change of mean hemispheric geopotential height if the time series had positive slope.) Figure 15a shows the January PNA pattern using 10-day data, while Figs. 15b–e depict the 10-day versions of the January TNH, January EU1, April NAO, and July SZ patterns, respectively. Figure 15d (the April NAO), in particular, should be compared to Fig. 2d in subsection 3a1.

Unauthenticated | Downloaded 08/21/22 12:56 PM UTC

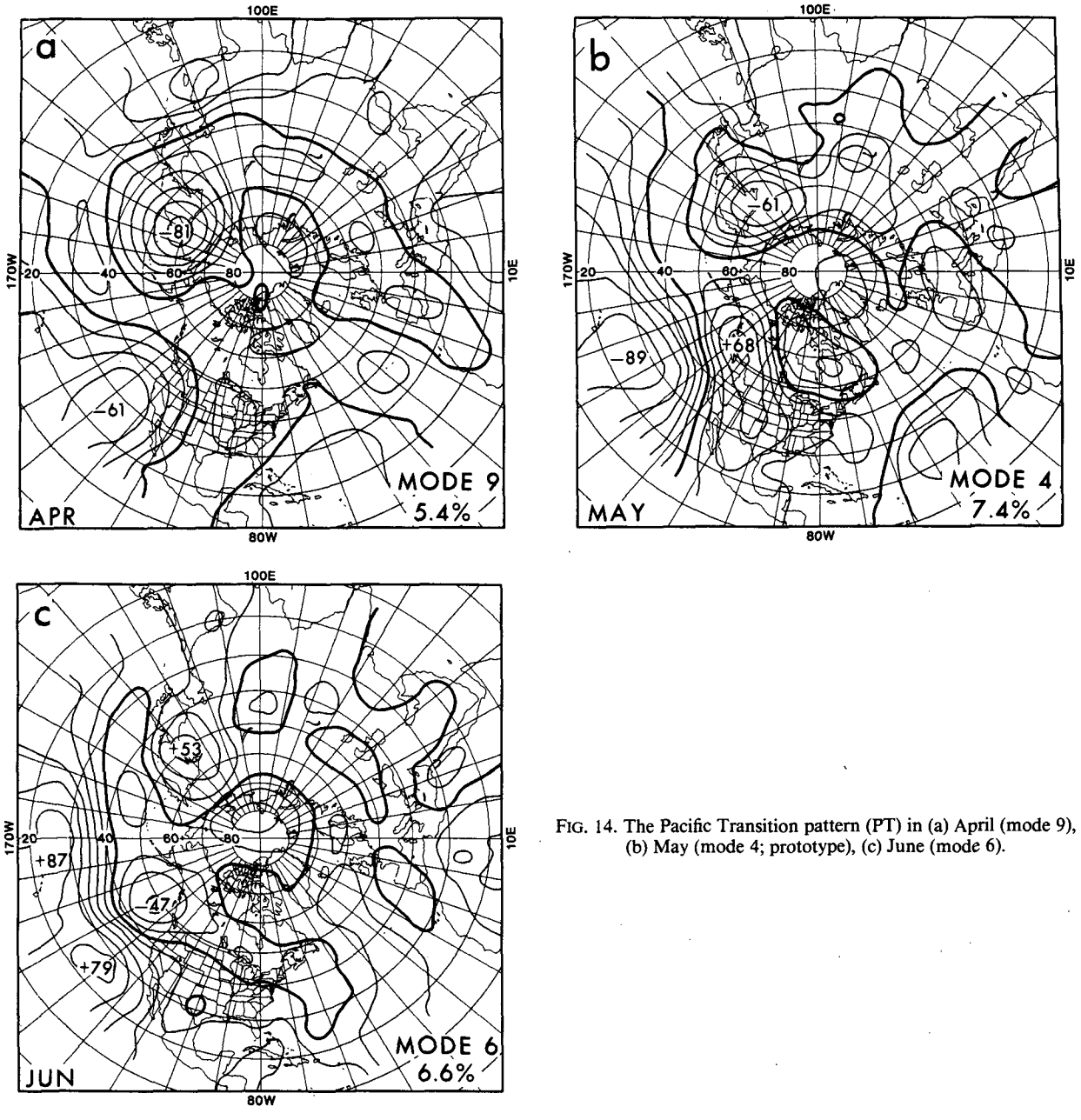

FIG. 14. The Pacific Transition pattern (PT) in (a) April (mode 9), (b) May (mode 4; prototype), (c) June (mode 6).

e. Persistence and transitions of 1- and 3-month circulation

Identification of the major quasi-independent modes of circulation for different times of the year is a first step toward prediction of the patterns. Some idea of the predictive potential is gained by examining lag correlations among the principal component time series associated with the modes. When the time series are lagged by a given number of months but matched by year, significantly nonzero correlations represent a predictive relationship between earlier and later associated patterns. When the patterns whose principal components are lag-correlated are alike, a systematic persistence or antipersistence of the pattern is suggested. It was considered desirable to examine pattern persistence allowing the two versions of the pattern whose amplitudes are lag-correlated to differ slightly because of seasonal evolution. An alternative would have been to lag-correlate projections of each month onto a constant estimate of a prototype for the pattern. Although this would reduce the effects of sampling errors in month-to-month model definitions, it would not take authentic seasonal evolution into account.

Not only is a specifiable proportion of the 6600 lag-correlation coefficients ($120 \times 110/2$) expected to be significant by chance, but the correlation required for

Unauthenticated | Downloaded 08/21/22 12:56 PM UTC

a given significance level increases as a function of year-to-year autocorrelations within individual time series which reduce the effective degrees of freedom (Livezey and Chen, 1983).

The results reveal about as many significant coefficients at the 0.05, 0.01 and 0.001 levels as would be expected by chance for both the 1- and 3-month averaging periods after accounting for interannual autocorrelation within series. Hence collective significance is not achieved and individually significant coefficients are regarded as accidental.

Because the persistence/recurrence results by themselves appear somewhat more promising, they are tested again in a small set of computations in which only the principal component time series for like patterns listed in Tables 2 and E1 between consecutive independent months or independent seasons (3-month-apart 3-month periods) are correlated, yielding a total of only 70 coefficients for the 1-month RPCs and 47 for the 3-month RPCs. Only a few (3 or 4 for monthly, 2 or 3 for seasonal) 0.05-significant coefficients are expected by chance, with 0 to 1 0.01-significant coefficients for each analysis group. Tables 4a and 4b show the coefficients resulting from this analysis applied to 1- and 3-month RPCs, respectively, where asterisks are used to denote significance levels in which interannual autocorrelational effects in the time series are partially taken into account following Livezey and Chen (1983). While this approach is not rigorous (Thiebaux and Zwiers, 1984), we believe it will allow us to evaluate the significance of this portion of our work reasonably. The coefficients in Tables 4a and 4b are shown by the precursor month (or season) rather than the target (predictand) month (or season). For example, 0.23 is the coefficient for predicting February PNA from January PNA. The symbol "×" denotes months or seasons in which the pattern is active only in the leading month/season. The signs of the coefficients take the polarity of the RPCA patterns into account, such that a positive sign reflects persistence of pattern polarity. Note that in the case of the 3-month results there are actually only one-third as many strictly independent coefficients as are shown in Table 4b; the superfluous entries are given in order to identify maxima or minima in the time variation of the indicated persistence more easily.

Several times the chance-expected number of 0.05- and 0.01-level significant coefficients occur both for monthly and seasonal persistence; thus, there is collective significance and many of the individual instances of persistence are likely to be significant.

Both 1- and 3-month results show more persistence than antipersistence, with the only noteworthy antipersistence occurring in the transition seasons. Persistence is most evident in the cold half of the year and in the SZ pattern, which applies to the lowest latitudes and easily shows the strongest persistence of any pattern in the study. All of these results are consistent with the point-by-point month-to-month 700 mb height lag correlation study of van den Dool and Livezey (1984). The SZ pattern is more persistent for the 3-month than the 1-month RPCs, so it also operates on an interseasonal time scale. It should also be noted that the interannual persistence of SZ is also quite marked.

The West Pacific Oscillation (WPO) shows the second highest amount of persistence, with roughly equal strength in the monthly as in the seasonal RPCs. Other patterns showing signs of persistence are the NAO, PNA, EU1, PT and NP patterns. The EA, EP and TNH patterns show significant persistence only for the January to February interval. Note that the NAO shows significant antipersistence from April to May, but that the 3-month RPCs do not indicate that phenomenon in late spring. The April to May NAO persistence relationship is complicated by the fact that the April RPCA pattern (Fig. 2d) is not highly representative of the prototypical NAO (note parentheses around the April NAO entry in Table 2), such that the lag correlation was computed between principal component time series associated with patterns that are only roughly similar. Nevertheless, each pattern broadly depicts a large-scale, north–south dipole over the central North Atlantic, and the reversal in sign of the respective

TABLE 3. Correspondence of 10-day mean with 1-month mean 700 mb height RPCA results. Parentheses indicate only an approximate correspondence.

January			April			July			October		
10-day mode	Pattern	Found in 1-month RPCA?	10-day mode	Pattern	Found in 1-month RPCA?	10-day mode	Pattern	Found in 1-month RPCA?	10-day mode	Pattern	Found in 1-month RPCA?
1	NAO	yes	1	NAO	yes	1	SZ, PT	yes	1	PNA	yes
2	WPO	yes	2	WPO	yes	2	—	yes	2	(EU2)	yes
3	PNA	yes	3	(annual cycle)	no	3	NAO	yes	3	NP, NA	yes
4	EP	yes	4	EU1	yes	4	AS	yes	4	NAO	yes
5	EA	yes	5	(EU2)	yes	5	—	yes	5	(annual cycle)	no
6	—	no	6	PNA	yes	6	—	yes	6	SZ	yes
7	EU1	yes	7	PT	yes	7	—	yes	7	EU1	yes
8	EU2	yes	8	(NP-like)	no	8	—	yes	8	—	no
9	TNH	yes	9	EA	yes	9	—	no	9	—	no
10	—	no	10	—	no	10	—	yes	10	—	no

Unauthenticated | Downloaded 08/21/22 12:56 PM UTC

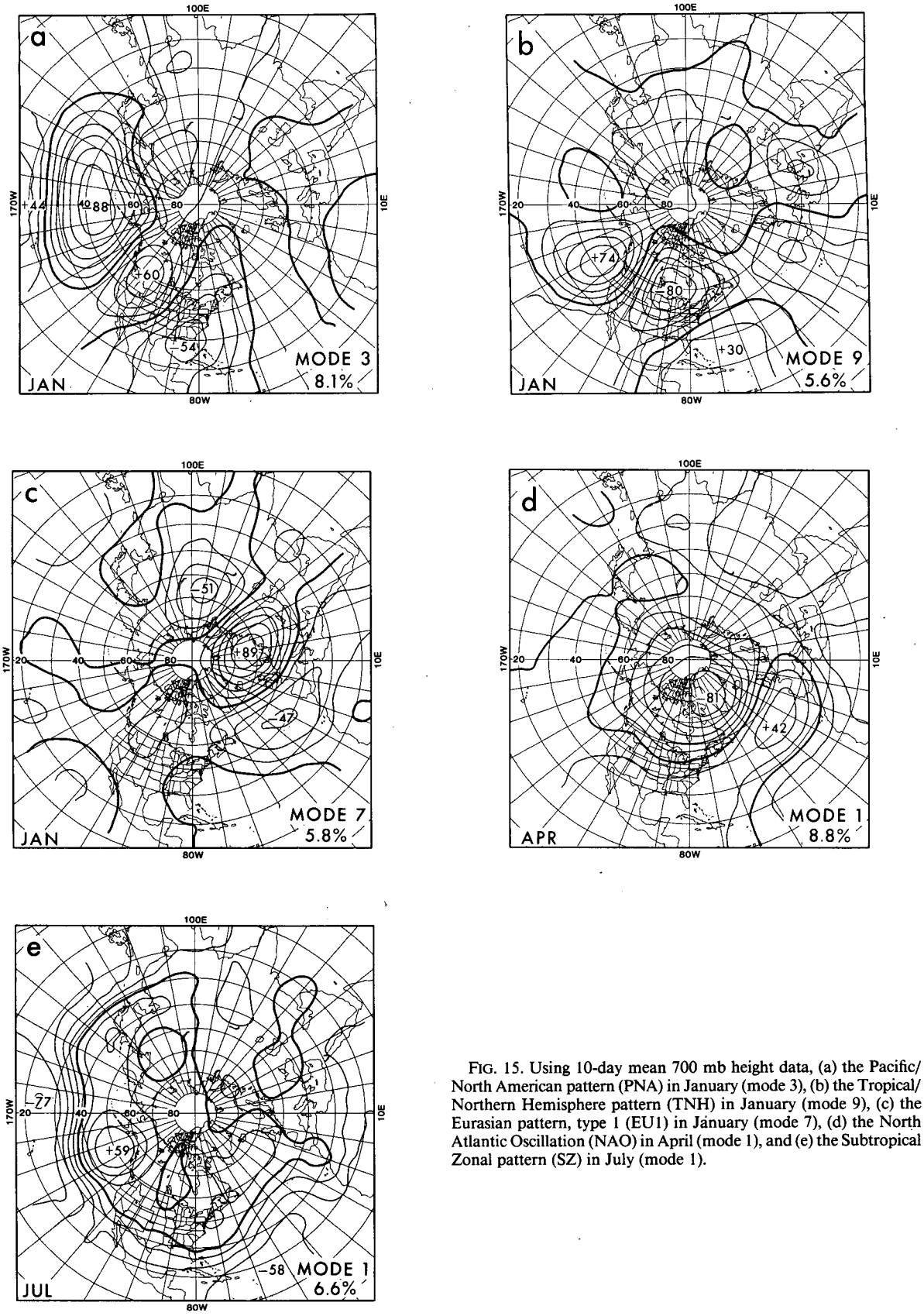

FIG. 15. Using 10-day mean 700 mb height data, (a) the Pacific/North American pattern (PNA) in January (mode 3), (b) the Tropical/Northern Hemisphere pattern (TNH) in January (mode 9), (c) the Eurasian pattern, type 1 (EU1) in January (mode 7), (d) the North Atlantic Oscillation (NAO) in April (mode 1), and (e) the Subtropical Zonal pattern (SZ) in July (mode 1).

Unauthenticated | Downloaded 08/21/22 12:56 PM UTC

TABLE 4a. Persistence statistics (correlations between rotated principal component time series) for 1-month mean 700 mb heights. Tabulated for precursor month.

Month	NAO	PNA	WPO	TNH	NA	EU1	EU2	EA	EP	SZ	AS	NP	PT
Jan	0.24	0.23	0.25	0.45*	0.04	0.10	0.09	0.33*	0.38*				
Feb	0.30	−0.02	0.33*	×	0.08	0.17	0.02	0.22	0.16				
Mar	−0.12	0.09	0.56*		×	0.15	×	0.00	×	0.56**			
Apr	−0.51*	×	0.11			0.11		×		×		0.34*	0.41*
May	0.27		×			×						0.01	0.42
Jun	0.03									0.33	0.22	×	0.33
Jul	0.26									0.46**	0.32		×
Aug	−0.05									0.16	×		
Sep	0.23	0.05				0.06	0.02			0.39*		0.16	
Oct	0.22	×			0.25	0.33	−0.11			×		×	
Nov	0.18		0.01	−0.24	−0.20	0.35	0.12	0.33					
Dec	0.37*	0.38*	0.26	0.28	−0.06	0.41*	0.20	0.14				×	

* Significant at 0.05 level.
** Significant at 0.01 level.
2-tailed test; uses effective df, based on autoregressive properties.

principal components occurred in 26 out of the 35 years examined. Consequently, it is hard to dismiss this antipersistent relationship as a statistical accident.

4. Robustness of the RPCA solutions

Many of the low-frequency circulation patterns obtained in this study have important meteorological implications. Some of them, especially during the nonwinter periods, have not been noted in other formal studies; this is also the case for information about all of the patterns' seasonalities. A question that naturally arises is whether all the results are authentic—i.e., whether the patterns are physical structures rather than mathematical or sampling artifacts that would be difficult to find on a particular chart or disappear with the addition of a sufficient number of new years to the record. This section addresses such questions from several independent vantage points.

a. Consistency within the present study

As emphasized in the beginning of section 3, one of the most compelling reasons for our confidence in the patterns that have been presented is their replication in three or more essentially independent RPCAs (Table 2). In order to establish that the similarity of the month-to-month realizations of a given pattern is much greater than that between the different patterns, spatial correlations among all maps were computed and the correlation of a pattern prototype with the chosen realization of that pattern for another month was compared with the prototype's correlation with the nine other possible maps for that month.

In 64 of the 68 possible such examinations, the correlation with the chosen map is the highest of the ten possibilities for the month in question, while in the other four cases it is the second highest by a small margin. Two of the four cases involve the NAO, one the PNA and one the SZ pattern. In one of the NAO cases (prototype versus August) and the PNA case (prototype versus September), this is simply a consequence of seasonality in the pattern form: the PNA wavelength is shorter in fall than in winter and the NAO contracts northward during summer. The other NAO case is with the February version, where the unclassified mode 5 yields a slightly higher correlation than the chosen

TABLE 4b. As in Table 4a except for 3-month mean 700 mb heights.

Season	NAO	PNA	WPO	TNH	NA	EU1	EU2	EA	SZ	AS	NP	PT
DJF	−0.07	0.01	0.21	×	×	−0.01	×	0.08				
JFM	0.34*	×	0.51**	×	0.04	−0.04	×	0.04				
FMA	0.27	×	0.25	×					0.53**			
MAM	0.18	×	×			×		×	0.71*		0.20	
AMJ	0.08		×		×	×		×	0.47*		0.29	
MJJ	0.31*		×						0.49*		0.25	×
JJA	−0.07								0.50*	×	0.46*	×
JAS	−0.07								×	×	0.26	
ASO	0.05					0.00	−0.04		×	×	−0.06	
SON	0.03	0.39*				−0.29	−0.13		×		×	
OND	−0.02	0.10	0.08		0.00	0.30*	−0.12	0.04			×	
NDJ	−0.04	−0.09	0.46*	0.07		×	×	×			×	

Unauthenticated | Downloaded 08/21/22 12:56 PM UTC

mode 2. The somewhat unique situation surrounding these two February patterns will be discussed in section 4c. Finally, in the SZ case the unclassified October pattern yielding a higher correlation with the prototype (July) than the chosen pattern has matching features irrelevant to the SZ pattern's basic definition.

It is clear that, overall, intrapattern strongly exceeds interpattern similarity. This would be evident to an even greater extent if a pattern's systematic seasonal changes were accounted for in this exercise. In fact, these continuous and physically reasonable month-to-month changes, either in the gross patterns' details or the relative strengths of their signals, constitute another form of consistency. One of the most dramatic examples of this is the seasonality of the PNA that is so clearly shown in Fig. 3.

Last, almost every pattern classified in the monthly mean data was replicated in the 3-month mean analyses (Table E1) and in the 10-day mean analyses for the four months that were examined (Table 3). The effective sample sizes for the 10-day analyses were probably more than twice those for the monthly RPCAs but considerably more variance from intraseasonal fluctuations (because of the weaker time filter) as well as the annual cycle had to be accommodated in the former.

b. *Consistency with other studies*

In section 3, the robustness of this study's results was implicitly treated in the form of their consistency with those of other studies, despite substantial differences in the analysis methods, periods of record, time filters, concatenations (or poolings) of the sampling elements, grids and datasets (appendix B). In particular, results are consistent with the three other RPCA studies (H81, HW and LT). Despite the use of the Harris-Kaiser II oblique rotation method in LT in contrast to our orthogonal varimax rotation, along with their coarser grid, shorter averaging period, broader data window, no data preprocessing, and an annual cycle to account for, the two sets of solutions are remarkably similar. In the January results, for example, even the one RPC loading pattern that was not acknowledged as a meteorological pattern (our mode 9) was also produced in LT, along with the excellent correspondences of the nine other patterns that are of greater interest. The LT components were reported to be nearly temporally orthogonal despite the use of a method that permits obliquity.[4] In fact, LT's results were quite insensitive to choice of several different rotational methods (see Richman, 1986, for a description and comparison of a number of oblique approaches). This suggests that the physical modes are indeed largely temporally orthogonal (as we presumed at the outset), such that an orthogonal rotation would not noticeably distort the natural relationships. Further support for the present results lies in their close agreement with H81's 15-year analysis. Despite a shorter record, coarser grid, pooling of winter months, uncorrected subtropical data and a slightly different application of the varimax method (i.e., normalization for variance explained among grid points; Horel, 1985, personal communication), those results contained six of the nine patterns classified here for January without ambiguity and the other three with only moderate distortion. Two of these last three were reproduced with good correspondence in the 30-year analysis in H81, but only five of the nine were found overall. Clues to why this occurred—that is, our success in confirming H81's 15-year results with a longer record when H81 found it not possible to do so—are provided in H81's narrative and his Fig. 5a. In the figure, modes 4 and 6–8 have a single center in the subtropics while mode 9 has its center over the Tibetan Plateau. Different grids were used in the two different analyses in H81. Apparently in switching from the WG gridded set to a subset of the NMC octagonal gridded set, some data contamination was introduced, particularly in the subtropics. It should be noted at this point that the WG grid is a subset of the NMC 541-point "diamond" grid in which, among other things, grid points south of 20°N have been omitted. One possibility for the contamination is that the diamond gridded set and the octagonal gridded set available to H81 may have been produced from different combinations of analyses.

In the current study, the diamond grid is also used and data points having suspected problems were either omitted (see section 2) or carefully corrected (see appendix A). Consequently, we are able to affirm H81's 15-year analysis and state that it was remarkably informative despite the record and grid limitations.

c. *Sensitivity of results to removal of parts of the period of record*

To examine the question of robustness versus degeneracy of the results more closely, the RPCA was repeatedly rerun on the 700 mb heights where each one of the 35 years (one year at a time) was omitted. Then pattern correlations between the resulting 34-year patterns and the corresponding 35-year patterns were computed. The results of this exercise are presented in Table 5 for the 1-month RPCA solutions. (Results for 3-month patterns are not shown.) The table is constructed similarly to Tables 2 and E1, except that the entries for each pattern for a given month show the average of the 35 correlation coefficients correlating each of the patterns produced from only 34 years with the full-sample pattern. The two numbers separated by a comma below the average correlation figure indicate the number of correlation coefficients out of the 35 that were below 0.90, followed by the number below 0.70 (if a coefficient is below 0.70, it is also indicated

[4] No two components were ever correlated over 0.3; over 90% of them were correlated less than 0.1.

Unauthenticated | Downloaded 08/21/22 12:56 PM UTC

to be below 0.90). These statistics are also given for the meteorologically unclassified modes on the right side of the table.

Any pattern with an average 34- versus 35-year correlation of less than 0.95 is considered rather unstable, as is any pattern having one or more instances of below 0.70 correlations.[5] The occurrence of a few such low correlations indicates that the pattern's integrity rests on a few extreme years in the sample and does not occur routinely during its indicated season. Some of the pattern stabilities in Table 5 clearly are weak, such as the 1-month NAO in April. They are still included in the classification because they closely resemble their adjacent month counterparts (unless parentheses are found around the mode number), at least one of which shows acceptable robustness. Several patterns having 2 to 4 months in their annual cycle were rejected because of unacceptable overall robustness/stability as defined in this exercise.

The tests described above were repeated for the 1-month RPCA results, except that now the seven sets of nonoverlapping consecutive 5-year groups were omitted, leaving seven 30-year samples. The outcome is shown in Table 6 in the same format as Table 5. Average correlations with full-sample patterns are now lower; 0.90 appears to be a reasonable threshold for robustness, and the occurrence of one or more of the seven correlations below 0.70 remains a caution signal.

As might be expected, the patterns occurring on leading mode numbers and having long seasonal cycles tend also to show great statistical stability, such as the NAO, PNA and WPO patterns during winter. The summer and transition patterns are comparatively less stable. The cold season EU1 and EU2 patterns appear to be adequately robust near the beginning and end of their seasonal cycles but less so during the winter, suggesting that they have transition pattern characteristics despite the centers of their cycles being in winter. Perhaps EU1 and EU2, the most extensive and zonally oriented continental of any of the patterns, are less geographically fixed during midwinter.

Most of the unclassified RPCA loading patterns have poor stability; however, a few actually appear to be as robust as some of the major winter patterns. Examination of the loading patterns reveals that while some of these isolated "signals" are probably statistical accidents, several appear to be variants of classified patterns in months when the chosen version of the pattern is somewhat deviant from its usual position and the unclassified but robust pattern serves to complement the first pattern. An example of this is shown in Fig. 16, where the chosen NAO pattern for February (mode 2; Fig. 2b) is somewhat different from the modal NAO in that the southern center is displaced to northern Europe and the zero-line is no longer approximately east–west. The unclassified mode 5 (Fig. 16a) is comparably robust (see Tables 5 and 6) and "fills in" the deficit in the mode 2 NAO. When the two patterns are averaged (after adjusting for the opposing polarities) a highly prototypical NAO is produced (Fig. 16b). An attempt to understand this partitioning of the NAO led to the realization that February's mode 5 was in fact a mixture of the central Atlantic NAO center and an unclassified, robust pattern that was replicated in the March RPCA as mode 2 (see Tables 5 and 6). This pattern is characterized (see Fig. 16a) by opposite signed centers in the central Atlantic and near Iceland.

Another instance of a robust unclassified pattern (March mode 8) is a secondary version of the WPO moved to the northwest from the position of the prototypical WPO pattern. In another case (August mode 3), an EU2-like pattern appears during the summer when EU2 is normally inactive. In both cases, we are probably looking at real manifestations of the atmosphere rather than artifacts of the RPCA. Instances of the latter, which are usually found in higher-order modes, are often identifiable by a meteorologically unplausible appearance in the pattern, such as two strong centers with great distance between them containing near-zero loadings. Such nonphysical patterns can result from "noise" in the analysis when most of the physical signal is contained in the preceding stronger modes.

The 5-year truncated record length tests were applied to the unrotated as well as rotated 1-month PCA solutions to illustrate Richman's (1986) observation that rotated PCs are less vulnerable than unrotated PCs to degenerate blending with neighboring components when using small samples. The resulting mean correlations between seven 30-year sample results and the full 35-year sample results for each month for the average of the ten modes are shown in Table 7. The rotated components consistently show the greater stability.

As another way of distinguishing the character of the unrotated from the rotated 1-month PCs, a comparison with associated teleconnection patterns was carried out in which the teleconnection base point was chosen as the point having highest amplitude on the RPCA loading pattern (Richman and Lamb, 1985). The resulting teleconnection pattern was then spatially correlated with the RPCA loading pattern from which its base point was derived. Pooling all 12 months for the ten modes, the average correlation between the unrotated PC loadings and associated teleconnections is 0.69 while for the rotated case it is 0.90. The average across the ten modes varies very little from month to month for both unrotated and rotated cases, being slightly higher in summer for the unrotated averages and higher in winter for the rotated. The major difference between the grand averages underlines the fact that the unrotated components contain more variance

[5] The 0.95 threshold was chosen subjectively on the basis of what was considered to represent a high degree of visual similarity. Correlations of 0.95, 0.90 and 0.70 approximately represent 90, 80 and 50% explained variance, respectively.

Unauthenticated | Downloaded 08/21/22 12:56 PM UTC

TABLE 5. Robustness of 1-month RPCA solutions with 1-year truncations of the 35-year input data. Top number is average correlation (times 100) of the 35 34-year patterns with full sample pattern; below this is the number (out of 35) of correlations below 0.90 and below 0.70. Hyphens and parentheses used as in Table 2.

														Unclassified patterns by mode number										
Month	NAO	PNA	WPO	TNH	NA	EU1	EU2	EA	EP	SZ	AS	NP	PT	1	2	3	4	5	6	7	8	9	10	
Jan	-99- 1, 0	99 0, 0	99 0, 0	-98- 1, 0	-99- 0, 0	97 4, 0	-93- 9, 3	97 2, 0	96 5, 0													91 12, 2		Jan
Feb	99* 0, 0	-99- 0, 0	99 0, 0	95 6, 0	98 2, 0	(89) 12, 5	99* 0, 0	-99- 0, 0	-95- 5, 1									98 0, 0				94 4, 1		Feb
Mar	100 0, 0	98 0, 0	99# 0, 0		98* 1, 0	(98)* 1, 0	99 1, 0	93 7, 1	97 3, 0	99# 0, 0					99 0, 0						99 1, 0		98 2, 0	Mar
Apr	(81) 29, 1	86 18, 3	94* 6, 1			97 2, 0		99 0, 0		94* 6, 1		82 24, 2	92 5, 2				98 0, 0	82 15, 10					77 30, 9	Apr
May	99 1, 0		96 7, 0			97 2, 1						-98- 1, 0	-98- 1, 0					98 0, 0		96 3, 0	93 6, 4	93 9, 0	95 3, 1	May
Jun	99 0, 0									(98)* 0, 0	98 1, 0	95 5, 1	98* 0, 0			97 1, 0	97 2, 0			96 4, 0	96 3, 1	95 4, 2	90 12, 2	Jun
Jul	99 0, 0									-96*- 6, 0	-98- 0, 0		(96)* 6, 0			96 4, 0		97 2, 0	97 3, 0	95 3, 1	89 11, 5	95 5, 1	96 3, 2	Jul
Aug	97 2, 0									96 6, 0	93 9, 0					96 4, 0	93 10, 1	96 4, 0		83 21, 6	90 13, 2	90 11, 5	90 12, 1	Aug
Sep	98 0, 0	99 0, 0				(94) 6, 1	99 0, 0			92 12, 2		96 2, 1					90 12, 1				87 14, 6	91 12, 0	94 6, 2	Sep
Oct	99 0, 0	99 0, 0			99* 0, 0	99 0, 0	99 0, 0			98 1, 0		99* 0, 0								97 1, 0	98 0, 0	96 5,0	89 8, 5	Oct
Nov	98 0, 0		99 0, 0	87 18, 5	89 13, 3	-99- 0, 0	92 8, 2	85 14, 9									99 0, 0	94 7, 0		97 3, 0				Nov
Dec	99 0, 0	97 0, 0	-96- 2, 0	92 6, 3	90 16, 0	89 13, 4	86 16, 8	96 5, 0				97 1, 0											79 26, 9	Dec

* Mode shared by two classified patterns in given month; both have symbol.

Same as * except for a second shared mode for the given month.

Unauthenticated | Downloaded 08/21/22 12:56 PM UTC

TABLE 6. As in Table 5 but for 5-year truncations, creating seven 30-year patterns to correlate with full sample pattern.

														Unclassified patterns by mode number										
Month	NAO	PNA	WPO	TNH	NA	EU1	EU2	EA	EP	SZ	AS	NP	PT	1	2	3	4	5	6	7	8	9	10	
Jan	-92- 3, 0	94 1, 0	94 2, 0	-90- 3, 1	-93- 1, 0	75 5, 3	-78- 6, 2	87 6, 0	74 6, 2													67 7, 4		Jan
Feb	94* 1, 0	-96- 1, 0	96 0, 0	84 6, 0	88 3, 1	(68) 6, 5	94* 1, 0	-96- 0, 0	-87- 3, 0									94 1, 0				73 5, 3		Feb
Mar	98 0, 0	88 3, 0	91# 2, 0		89* 2, 1	(89)* 2, 1	95 1, 0	75 5, 2	90 3, 0	91# 2, 0					90 2, 1						92 1, 0		81 3, 2	Mar
Apr	(82) 4, 1	86 5, 0	87* 3, 1			86 5, 0		94 2, 0		87* 3, 1		80 5, 1	77 6, 2				91 1, 1	88 4, 0					66 7, 5	Apr
May	94 1, 0		89 3, 0			89 3, 1						-90- 1, 1	-88- 3, 0					90 2, 0		81 6, 1	81 4, 2	76 5, 2	82 3, 2	May
Jun	97 0, 0									(90)* 2, 0	86 5, 0	83 4, 2	90* 2, 0			86 4, 1	85 3, 1			86 3, 1	75 7, 2	81 4, 2	66 6, 3	Jun
Jul	95 0, 0									-87*- 4, 0	-91- 3, 0		(87)* 4, 0			86 4, 1		82 5, 2	83 5, 1	80 4, 2	70 7, 4	85 4, 1	84 6, 0	Jul
Aug	94 1, 0									88 3, 0	87 5, 0					93 2, 0	84 3, 2	86 5, 1		78 6, 1	86 4, 0	82 5, 1	75 6, 3	Aug
Sep	85 3, 1	95 1, 0				(84) 5, 0	95 1, 0			79 4, 3		82 4, 1					81 4, 1				79 4, 2	72 7, 2	79 5, 2	Sep
Oct	96 0, 0	95 1, 0			94* 2, 0	92 1, 1	95 1, 0			86 4, 0		94* 2, 0								84 4, 2	82 4, 2	88 3, 1	64 7, 4	Oct
Nov	93 1, 0		96 0, 0	82 6, 1	66 7, 4	-95- 1, 0	81 4, 2	86 3, 1									89 2, 1	87 3, 0		91 3, 0				Nov
Dec	97 0, 0	89 3, 0	-92- 3, 0	85 4, 0	84 4, 0	82 6, 1	83 5, 1	91 3, 0				94 2, 0											65 6, 3	Dec

* Mode shared by two classified patterns in given month; both have symbol.
# Same as * except for a second shared mode for the given month.

Unauthenticated | Downloaded 08/21/22 12:56 PM UTC

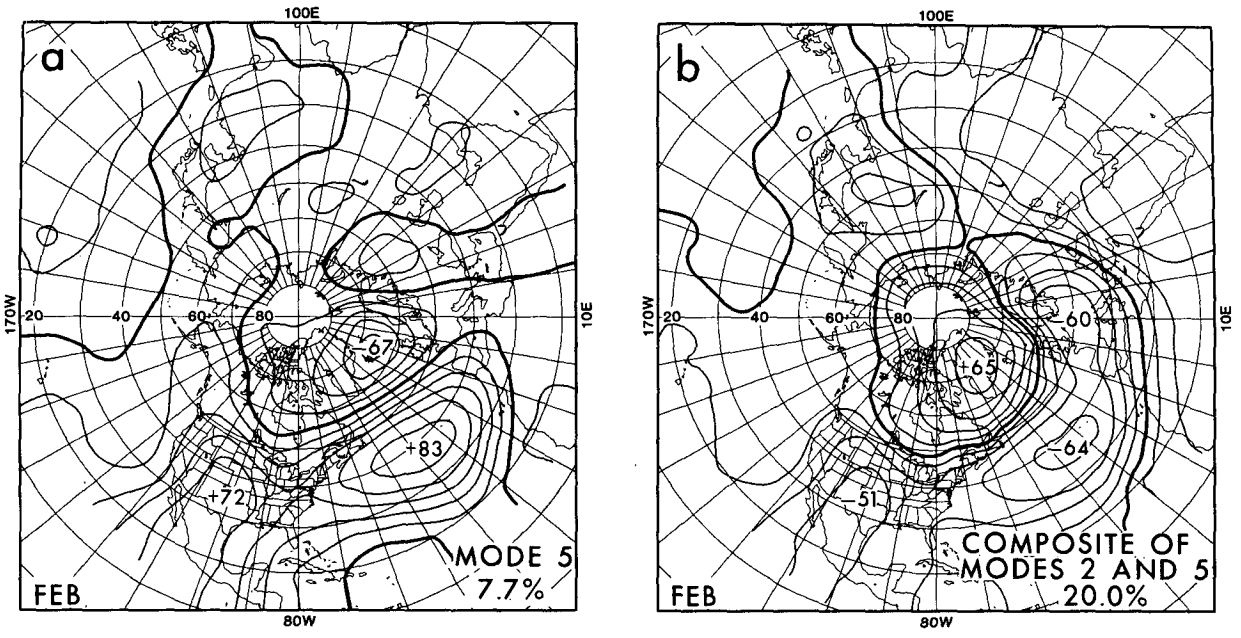

FIG. 16. The February mode 5 pattern (unclassified, but NAO-like) shown in (a) is combined with the classified February mode 2 NAO pattern shown in Fig. 2b to obtain the exemplary NAO pattern as the composite, shown in (b).

than that associated with a single correlational complex in the input data. As might be expected, the correlations for leading modes tend to be higher than for higher order modes, and for classified patterns higher than for unclassified patterns. The correlations for some of the strong rotated winter patterns are in the upper 0.90s such that the teleconnection map is virtually indistinguishable from the RPCA loading map except for the base point center having unrealistically high relative amplitude in the former. In general, the rotated patterns with very high correlations with their teleconnection counterparts are the ones that fared well in the robustness examinations described above. The January TNH pattern was among those exhibiting such a high correlation, showing that its failure to be acknowledged in past teleconnection studies is not attributable to a lack of reproducibility, but rather to the practice of choosing the teleconnection patterns on the basis of the strength of the primary negative correlation with the base point. There may be no single objective method of selecting base points for teleconnections that would produce the same patterns as those resulting from RPCA.

5. Discussion

Because this study exploits a well-resolved, approximately uniformly dense grid for the virtually maximum possible period of record, for homogeneous monthly mean data that are largely free of major problems (section 2 and appendix A), we feel the resulting descriptions of the form and seasonality of low-frequency circulation variability (section 3) can reasonably be regarded as useful benchmarks against which other descriptions might be compared. In this regard, the process of classifying the major monthly mean 700 mb circulation patterns has helped to tie the results of other recent teleconnection and RPCA studies of the quasi-stationary flow together (section 3 and appendices B–D).

The advantages of the use of RPCA have been argued at length (section 1), and these advantages demonstrated through the extensive validation of the principal results of its application (section 4). Consequently, the set of results here—patterns and accompanying time histories—form a complete, quantitative basis, in which individual components are physically realizable,

TABLE 7. Mean correlations for the first 10 modes between truncated record (30 out of 35 years) principal component patterns and full sample patterns by month for unrotated and rotated loading patterns. Seven truncations are simulated for each month-mode comparison.

	Unrotated	Rotated
Jan	83	84
Feb	83	88
Mar	80	89
Apr	79	84
May	80	86
Jun	77	84
Jul	76	84
Aug	80	85
Sep	77	83
Oct	79	88
Nov	80	87
Dec	82	86
Mean	80	86

Unauthenticated | Downloaded 08/21/22 12:56 PM UTC

for the low-pass filtered portion of flow variability. Such a basis should constitute an improved tool for sorting out relationships in the climate system between upper-air anomalies and other parts of the system. For example, the question of whether more skill is obtained when using screened gridded 700 mb height data or empirical orthogonal functions (EOFs) of the heights as multiple regression predictors for the specification of time-averaged surface temperatures (cf. Klein and Walsh, 1983; Walsh, 1984) may diminish in importance if RPCs are considered as well. A number of other possibilities for applications exist.

These potential studies as well as other future empirical studies using approaches other than RPCA might benefit from other lessons either reinforced or learned here. The first is that prescreening of data frequently uncovers obvious difficulties that can make the difference between detection and nondetection of desired signals (sections 2, 4b and appendix A). Next, there are important intraseasonal changes in both the form and relative importance of the patterns that make up low-frequency variability (section 3). Every effort should be made not to obscure these changes and distort subsequent patterns by combining data over a number of calendar months to build sample sizes. It appears that demands on sample size are less severe for RPCA than for unrotated PCA. The third and last point that we wish to note further ameliorates the problem of building adequate samples for analysis. This is that much shorter time averages (or a higher frequency cutoff filter), such as 10- or 15-day means, are all that are necessary to extract the crucial information about the quasi-stationary circulation (section 3d). It is not necessary to form 30-day or longer means, in the process discarding information obtainable through shorter period, but adequate, filters. In fact, when daily data are availabe it is preferable to filter those data (either with a running mean or a more sophisticated filter) and retain the entire series in the analysis (if appropriate). As long as it is well understood that such data are highly autocorrelated and consequently not independent, the maximum amount of information about the time scales of interest can be realized.

With respect to this last point it was noted in section 3e that lag correlational data relating rotated principal component time series did not convincingly demonstrate systematic transitions among patterns other than persistence/antipersistence of the same pattern. One possible reason for this failure might have been too short a record length to obtain a complete separation between the circulation patterns each month or season, even after rotation. However, if systematic transitions exist, a more likely reason for our failure to detect them is our use of a crude 30-day moving average filter with a sampling frequency of only once per month. A shorter averaging period (e.g., 10-day) with a sampling frequency of once per day applied over 45-day windows might permit the detection of the initial growth or final decay of quasi-stationary flow events. This would make possible the estimation of typical pattern lifetimes and probabilities of their occurrence, as well as interpattern transitions. Such a more detailed RPCA is currently in progress.

Acknowledgments. Much of the foundation on which this work was built was laid by John Horel at Scripps Institute of Oceanography and William Lebow of Scientific Systems, Inc. through their work, interest, and advice. Donald Gilman of the Climate Analysis Center has consistently supported our research objectives and scientific judgement over the course of this work. A number of individuals offered carefully considered, constructive critiques of earlier versions of the manuscript: Edward Epstein, Steven Esbensen, John Horel, Kingtse Mo, Reviewer B, Michael Richman, Chester Ropelewski, Huug van den Dool, John Wallace, and John Walsh. Kathy James assisted with typing and David Durdall with computer graphics, while drafting was done by Michael Gaidurgis with timely backup from Laura Rumburg.

APPENDIX A

Correction of the Carribean and North African 700 mb Data Problem in the 1950s

The presence of a data problem was first suggested in the rotated principal component analysis results for summer in H81, in which the loading pattern of the leading mode had a large isolated negative center in the Caribbean, a location which by itself is not known to have any particular meteorological significance in summer. The amplitudes associated with this mode were very low only up to the middle 1950s.

An examination of the interannual time series of 700 mb heights for each of the 358 grid points for each month uncovered some rather abrupt discontinuities in the middle 1950s in the Caribbean and North Africa, in which heights before the discontinuity point were higher and less variable than afterward. July showed the most severe such pattern, and for the largest number of grid points of any month. Figure 1 shows the locations of the 16 affected grid points in July. In other months, the affected points are subsets of these July points. An example of one of the discontinuous time series (expressed in standardized departures from the period mean) is provided in Fig. A1 for grid point number 16 (located at 20°N, 10°E) in July.

In order to identify the grid points involved in the problem, the mean of the standardized departures from the 35-year means for years prior to the discontinuity point were compared with that for the following years, and maps of the differences were examined. Only those points/months that were obviously (to us) affected were corrected. The positive bias appears to have occurred until 1956 in the Caribbean area and until 1958 in North Africa. Table A1 presents the numbers of meters (times 10) to be subtracted from the unadjusted heights

Unauthenticated | Downloaded 08/21/22 12:56 PM UTC

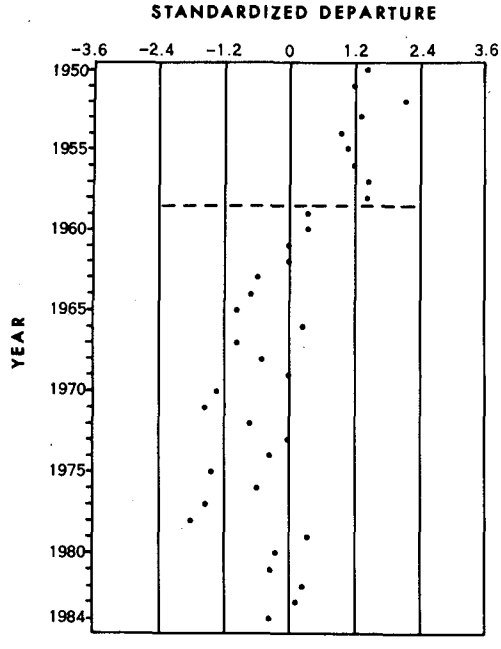

FIG. A1. The standardized departures from the 35-year mean of July 700 mb height for each of the 35 Julys for grid point number 16 in Fig. 1 (20°N, 10°E) before the 1950–58 bias correction.

at each of the 16 grid points for each month in order to adjust the 7- or 9-year mean at the beginning of the period to that for the remainder of the series believed to be bias-free. Apparent discontinuities in Table A1 (e.g., March through May for points 1 and 2) reflect both a reluctance to make adjustments where not obviously necessary and a lack of spatial and month-to-month smoothing of those that were made. A modest bias does seem to be present at points 1 and 2 for Aprils in the early 1950s, but the choice was made not to perform the adjustments there. Note that they were made at points 5–7 where it was felt the bias was large enough to warrant them.

The 700 mb heights at grid points over the central and south-central United States were above their average during many of the summer months in the 1950s due to a heat wave regime during that decade, but the behavior shown by these grid points is not similar to that of the ones over the Gulf of Mexico, Cuba and North Africa that are affected by the data problem.

The effect of the adjustment is quite noticeable in the July rotated principal component analysis. Figure A2 shows two of the loading patterns before (parts a and b, showing modes 2 and 4, respectively) and after (parts c and d, showing modes 2 and 8) the adjustment. Note that before the adjustment the Caribbean and North African data problem areas are strongly represented on mode 2 (Fig. A2a), combined with the genuine Subtropical Zonal (SZ) pattern in those same two regions (characteristic of the warm season at low latitudes), as well as the 1950's heat wave regime over the United States. The principal component time series (amplitudes) associated with this pattern are high in the early and middle 1950s, revealing the link with the subtropical data problem. Mode 4 (Fig. A2b) contains the Pacific and mid-Atlantic parts of the SZ pattern; only the normal amplitude level is found in the 1950s.

After the adjustment the SZ pattern occupies one mode (mode 2) instead of two (Fig. A2c), and its amplitudes are not higher in the 1950s than during the rest of the period of record. Mode 8 (Fig. A2d) is now bias-free, showing some of the non-SZ features (e.g., the North Atlantic region) shown in mode 2 before the correction. Its time series behaves normally in the 1950s. The rotated principal component analysis solutions before versus after the bias adjustment help to confirm that the adjustment was applied appropriately. Although the data problem may not be eliminated completely, its major amelioration helps provide a much less contaminated analysis, especially in summer.

Two final tests were performed to check the efficacy of the adjustments. RPCA was reperformed on unadjusted July data with the first 7 and 9 years withheld,

TABLE A1. Monthly adjustments ($m \times 10$) for each of the 16 grid points identified in Fig. 1, which are subtracted from the unadjusted 700 mb heights for 1950–56 in the Caribbean and for 1950–58 in North Africa.

	Grid point number (as shown in Fig. 1)															
	Caribbean								North Africa							
Month	1	2	3	4	5	6	7	8	9	10	11	12	13	14	15	16
Jan					145	144										
Feb	228	264			131	131										
Mar	218	252	207		134	177	149									
Apr					74	90	93	79								
May	115	154			84	111	105									
Jun	119	142	115		99	122	90				278	239			203	300
Jul	83	110	125	90	61	116	109	86	172	222	290	311	207	186	288	395
Aug	97	104				90	86		178		255	281	185		265	366
Sep			82			93	86			142	209	190				271
Oct							109									
Nov					87	116	71									152
Dec					83	124										

Unauthenticated | Downloaded 08/21/22 12:56 PM UTC

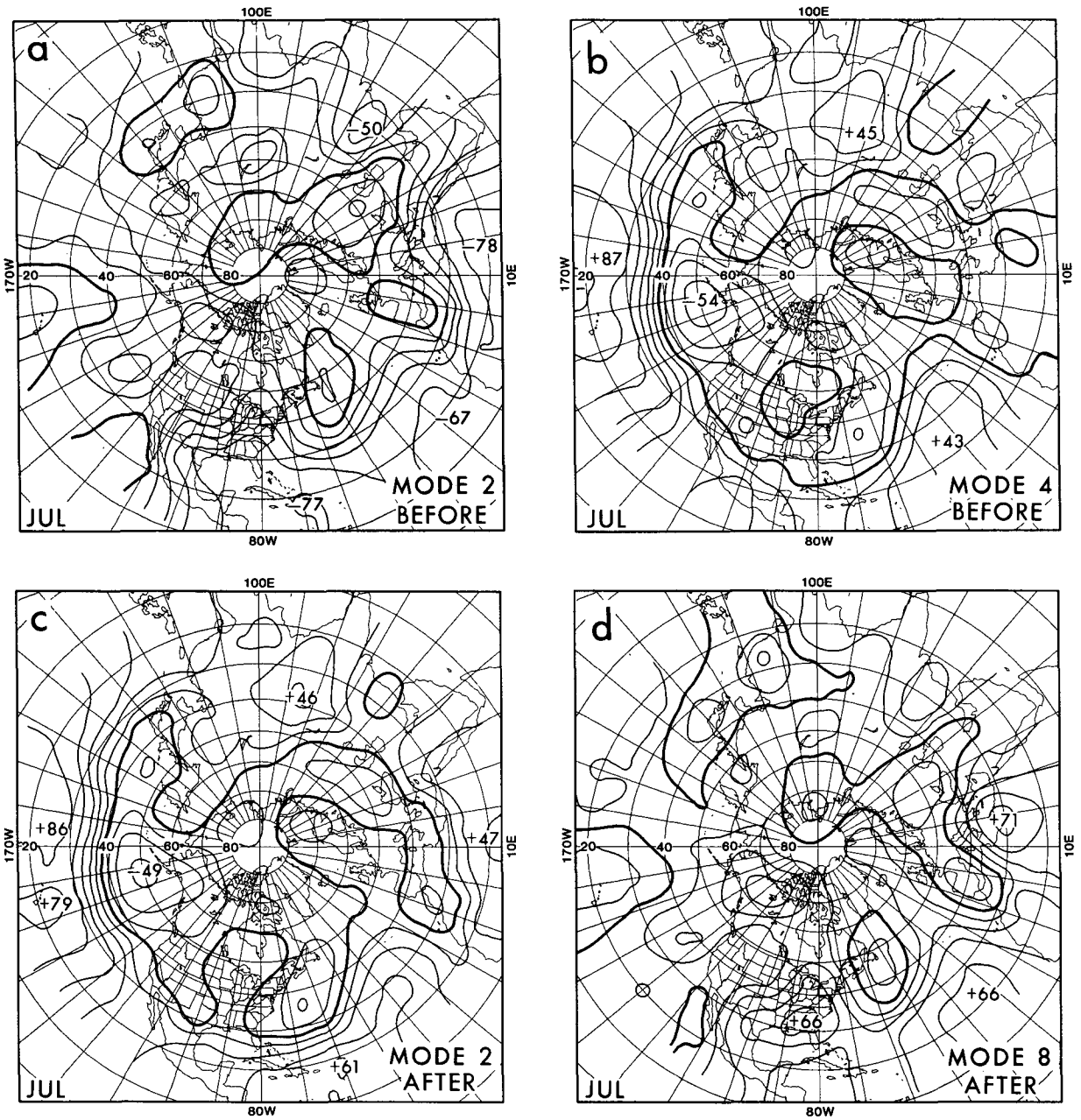

FIG. A2. Rotated principal component analysis solutions for July before (a and b) and after (c and d) correction of the low latitude data problem. See text for details.

respectively. If either or both of these analyses reproduce the essential features of the SZ pattern shown in Fig. A2c, our confidence in both the adjustments and the pattern reproducibility will be enhanced accordingly, though the latter is well-established in section 4c (see Tables 5 and 6). On the other hand, failure to pass either of these severe tests should not proportionately diminish our confidence because 20% and 26% reductions, respectively, are being made in an already small sample.

With the removal of 1950–56 Julys, the SZ pattern (Fig. A2c) was replicated closely as mode 4 (not shown) by the RPCA. Removal of two more years (for a sample size of only 26) leads to mixing and separation of the pattern between modes 1 and 3 (not shown). Specifically, loadings over the subtropical Pacific are split between the modes, with the subtropical Atlantic variance mainly residing in mode 1 and the North African variance in mode 3. In neither mode was the Pacific decoupled entirely from the Atlantic as in mode 2 for the full-period unadjusted RPCA (Fig. A2a). Consequently, these additional tests lend considerable support to the data correction procedures and summertime patterns presented here.

Unauthenticated | Downloaded 08/21/22 12:56 PM UTC

APPENDIX B

Winter Comparison of the Present Study's Orthogonally Rotated Principal Component Results with Results of Five Major Studies of Low-frequency Upper-air Variability in the Northern Hemisphere

	Barnston and Livezey (1987) (present study)	Wallace and Gutzler (1981) (WG)	Horel (1981) (H81)	
Analysis method, meteorological parameter	orthogonally rotated principal components of 700 mb height	teleconnections of 500 mb height	orthogonally rotated principal components of 500 mb height	
Grid	358-point approx. equal area (derived from NMC 541-point diamond grid)	111-point approx. equal area (derived from NMC 541-point diamond grid)	111-point approx. equal area (derived from NMC 541-point diamond grid)	120-point approx. equal area (every 4th point of NMC octogonal grid)
Source of data	NMC	NMC: obtained from NCAR	NMC: obtained from NCAR	NMC
Period of record	1950–84 (35 years)	1963–1977 (15 years), and 1950–1962 (13 years)	1963–1977 (15 years)	1951–1980 (30 years)
Averaging period per sampling element	1-month	1-month	1-month	1-month
Concatenation (pooling) time window; sampling elements per time window	1 month (Jan); 1	3 months (DJF); 3	3 months (DJF); 3	3 months (DJF); 3
Major preprocessing of data	treatment of early 1950s analysis bias in Caribbean and North Africa; exclusion of grid points in Himalayas, India, Saudi Arabia			
Names of robust January circulation patterns found in present study, with names of corresponding winter patterns found in the other studies	North Atlantic Oscillation (NAO) (mode 1: 11.1%)	Western Atlantic (WA)	mode 5 (6.1%)[1] mode 3 (7.3%)[2]	mode 10 (4.5%)
	Pacific/North American (PNA) (mode 2: 10.8%)	Pacific/North American (PNA)	mode 2 (8.7%)	mode 1 (7.8%)
	West Pacific Oscillation (WPO) (mode 3: 9.8%)	Western Pacific (WP)	mode 1 (12.9%)	mode 3 (6.1%)
	Tropical/Northern Hemisphere (TNH) (mode 4: 9.8%)		mode 5 (6.1%)[1] mode 6 (5.0%)[3]	mode 5 (5.5%)
	Northern Asian (NA) (mode 5: 8.3%)		mode 4 (6.9%)	
	Eurasian #1 (EU1) (mode 6: 8.0%)	Eurasian (EU)[1]	mode 8 (4.5%)[4] mode 10 (4.0%)	
	Eurasian #2 (EU2) (mode 7: 7.7%)		mode 9 (4.5%)	
	East Atlantic (EA) (mode 8: 5.8%)	Eastern Atlantic (EA)	mode 3 (7.3%)	mode 2 (7.0%)
	East Pacific (EP) (mode 10: 5.0%)		mode 7 (4.7%)	
Column footnotes		[1] Japanese center version	[1] is westward-displaced NAO and northeastward-displaced TNH without Pacific center [2] good as EA; also is southeast version of NAO [3] only 2 western centers appear: mode 5 provides some of Caribbean center [4] mode 8: Mongolian and Japanese centers mode 10: Scandanavian center	
Patterns not corresponding to any of those classified in present study				mode 4 (5.8%)* mode 6 (4.9%)* mode 7 (4.9%)* mode 8 (4.7%)* mode 9 (4.6%)** * Single, subtropical center ** Single, mid-latitude center

Unauthenticated | Downloaded 08/21/22 12:56 PM UTC

APPENDIX B (*Continued*)

Esbensen (1984) (E)		Lebow and Toldalagi (1985) (LT)	Hsu and Wallace (1985) (HW)
teleconnection of 700 mb height		obliquely rotated principal components of 700 mb height	500 mb height patterns associated with orthogonally rotated principal components of sea level pressure
541-point NMC diamond grid (36 points per latitude circle)		111-point approx. equal area (derived from NMC 541-point diamond grid)	1977-point NMC octagonal equal area
NMC		NMC	NMC: obtained from NCAR
1950–1977 (28 years)		1949–1982 (34 years)	1947–1977, without 1960, 1961 (29 years)
1-month		½-month	5-day
3 months (DJF); 3		2 months (mid-Dec. to mid-Feb.); 4	5 months (NDJFM); 30
digital filter to obtain intermonthly signal	digital filter to obtain interannual signal		
Western Atlantic (WA) Zonally-Symmetric Seesaw (ZS)*	Western Atlantic (WA) Zonally-Symmetric Seesaw (ZS)[1]	mode 2 (8.8%)	Atlantic pattern (A) (SLP mode 1: 7.3%)
Pacific-North American (PNA)	Pacific-North American (PNA)	mode 4 (7.0%)	Pacific/North American (PNA) (SLP mode 6: 4.8%)
Western Pacific (WP)[1]		mode 1 (8.9%)	Pacific pattern (P)[1] (SLP mode 3: 6.1%)
	Zonally-Symmetric Seesaw (ZS)[1]	mode 7 (5.8%)	
Northern Asian (NA)		mode 5 (6.1%)[1]	Siberian Pattern (S) (SLP mode 2: 6.1%)
Eurasian (EU)*[2]	Eurasian (EU)*[2]	mode 10 (4.3%)[2]	Chinese Pattern (C)[2] (SLP mode 4: 5.9%)
Eastern Atlantic (EA)[3]	Eastern Atlantic (EA)*[3] Zonally-Symmetric Seesaw (ZS)[1]	mode 9 (4.5%)[3]	
Eastern Atlantic (EA)[3]		mode 6 (6.0%)	unnamed; "N-S seesaw with major center over North Africa"[3] (SLP mode 5: 5.1%)
	North Pacific (NP)	mode 8 (5.7%)	
[1] less prominent U.S. center	[1] most strongly NAO, but clearly contains TNH and EU2 also	[1] strong European center also	[1] translated east
[2] Japanese center version	[2] Japanese center version	[2] all 4 centers represented	[2] only Mongolian and Japanese centers
[3] mixture of EA (Atlantic center displaced to east) and EU2 (eastern center displaced to northwest)	[3] mixture of EA (Atlantic center displaced to east) and EU2 (eastern center displaced to northwest)	[3] somewhat different (Caspian center shifted southwest, Chinese center shifted northwest, Pacific center appears)	[3] pattern not shown in paper
* interannual signal stronger	* intermonthly signal stronger		
		mode 3 (7.2%)	

Unauthenticated | Downloaded 08/21/22 12:56 PM UTC

APPENDIX C

As in Appendix B Except for Summer

	Barnston and Livezey, 1987 (present study)	Horel, 1981 (H81)	Lebow and Toldalagi, 1985 (LT)
Analysis method, meteorological parameter	orthogonally rotated principal components of 700 mb height	orthogonally rotated principal components of 500 mb height	obliquely rotated principal components of 700 mb height
Grid	358-point approx. equal area (derived from NMC 541-point diamond grid)	120-point approx. equal area (every 4th point of NMC octagonal grid)	111-point approx. equal area (derived from NMC 541-point diamond grid)
Source of data	NMC	NMC	NMC
Period of record	1950–84 (35 yrs)	1951–80 (30 yrs)	1949–82 (34 yrs)
Averaging period per sampling element	1-month	1-month	½-month
Concatenation (pooling) time window; sampling elements per time window	1-month (Jul); 1	3 months (Jun–Jul–Aug); 3	2 months (mid Jun–mid Aug); 4
Names of robust July circulation patterns found in present study, with names of corresponding summer patterns found in H81 and LT	North Atlantic Oscillation (NAO) (mode 1: 9.6%)	mode 5 (3.4%)	mode 4 (5.4%)
	Subtropical zonal (SZ)[1] (mode 2: 7.9%)	mode 2 (12.5%)[1] mode 3 (5.5%)[2]	mode 1 (8.2%)[1] mode 3 (6.0%)[2]
	Asian Summer (AS) (mode 4: 6.8%)	mode 7 (3.1%)[3]	mode 7 (4.1%)
	Pacific Transition (PT)[1] (mode 2: 7.9%)		mode 3 (6.0%)[2]
Column footnotes	[1] SZ and PT share mode 2; July final month for PT.	[1] Pacific sector [2] African sector [3] translated southeast	[1] Eastern Hemisphere, Atlantic [2] Pacific SZ and PT
Patterns not corresponding to any of those classified in present study		mode 1 (13.7%)[B] mode 4 (4.0%)** mode 6 (3.2%)* mode 8 (3.1%)** mode 9 (2.8%)** mode 10 (2.7%)*	mode 2 (6.8%)[B] mode 5 (5.1%)** mode 6 (4.3%)** mode 8 (3.6%)** mode 9 (3.5%)** mode 10 (3.2%)**

[B] contains 1950's data bias.
* Single low-latitude center.
** Midlatitude pattern with at least two centers.

Unauthenticated | Downloaded 08/21/22 12:56 PM UTC

APPENDIX D

As in Appendix B except for April and October. Analysis Specifications are Analogous to Those Shown in Appendix B for Barnston and Livezey and for Lebow and Toldalagi. Left Column for April or October Lists Patterns Found in the Present Barnston and Livezey Study, Right Column Lists Modes of Corresponding Patterns in Lebow and Toldalagi. Patterns Not Corresponding to Any Classified in Present Study at Bottom

April		October	
Barnston and Livezey	Lebow and Toldalagi	Barnston and Livezey	Lebow and Toldalagi
North Pacific (NP) (mode 1: 11.1%)	mode 8 (4.9%)[1]	North Pacific (NP) (mode 1: 10.6%)	mode 3 (5.8%)
Subtropical Zonal (SZ) (mode 2: 9.5%)[1]	mode 2 (7.6%) mode 4 (5.6%)[2] mode 5 (5.4%)[3]	Eurasian type 2 (EU2) (mode 2: 8.9%)	mode 7 (5.4%)
North Atlantic Oscillation (NAO) (mode 3: 8.3%)	mode 1 (7.8%)	Pacific/North American (PNA) (mode 3: 8.7%)	mode 2 (5.9%)
Pacific/North American (PNA) (mode 6: 6.6%)		Subtropical Zonal (SZ) (mode 4: 8.3%)	mode 5 (5.6%)
Eurasian #1 (EU1) (mode 7: 6.5%)	mode 10: (4.0%)	North Atlantic Oscillation (NAO) (mode 5: 7.4%)	mode 1 (6.0%)
East Atlantic (EA) (mode 8: 6.4%)	mode 3: (5.7%)	Eurasian #1 (EU1) (mode 6: 7.3%)	mode 4 (5.6%)
Pacific Transition (PT) (mode 9: 5.4%)	mode 5 (5.4%)[3]	Northern Asian (NA) (mode 1: 10.6%)	mode 8 (5.2%)[1]
West Pacific Oscillation (WPO) (mode 2: 9.5%)[1]	mode 4 (5.6%)[2] mode 5 (5.4%)[3]		
[1] good SZ; also contains WPO	[1] translated east [2] WPO and SZ mixture translated east slightly [3] WPO and SZ mixture translated northwest, plus PT		[1] contained in different pattern
Unclassified in present study	mode 6 (5.3%)** mode 7 (5.0%)** mode 9 (4.1%)**	Unclassified in present study	mode 6 (5.5%)** mode 9 (5.0%)** mode 10 (4.8%)**

** Midlatitude patterns with at least two centers.

Unauthenticated | Downloaded 08/21/22 12:56 PM UTC

TABLE E1. As in Table 2 but for 3-month mean 700 mb height.

	All	Cold season							Warm		Transition	
Season	NAO	PNA	WPO	TNH	NA	EU1	EU2	EA	SZ	AS	NP	PT
DJF	-1-	-2-	3	-4-	-7-	8	6	-5-				
JFM	1	(2)^{TNH}	3	(2)^{PNA}	7	-6-	(5)	(8)				
FMA	(1)	(2)^{TNH}	-3-^{SZ}	(2)^{PNA}					(3)^{WPO}			
MAM	1	(3)^{NP}	2^{SZ}			6		(7)	(2)^{WPO}		3^{PNA}	
AMJ	(1)		3^{SZ}		5	8		6	3^{WPO}		4	
MJJ	1		(4)						2^{PT}		(5)	-2-^{SZ}
JJA	1								4^{PT}	3	10	(4)^{SZ}
JAS	2								-1-	-4-	8	
ASO	3					9AS	6		4	(9)^{EU1}	-2-	
SON	3	7				2	8		1		4	
OND	1	5	7		(2)^{EU2}	3	-2-^{NA}	4			8	
NDJ	1	2	3	8		4	6	5			7	

APPENDIX E

Three-Month Mean Circulation Patterns

Repetition of RPCA using 3-month mean height data produces solutions similar to those for monthly means, with some modifications. Certain of the patterns that are distinct on the 1-month time scale tend to blend in the 3-month patterns while others lose some strength. A few 1-month patterns achieved greater stature in the seasonal results. Some seasonal patterns are similar to their 1-month counterparts, but have one or more of their features shifted in location slightly.

Unlike the 1-month solutions, the adjacent 3-month solutions overlap by two-thirds so that the occurrence of a given pattern in such periods no longer constitutes mutually independent pattern validation, which now requires pattern similarity in analyses centered 3 months apart. This presents a problem for patterns whose active period is only 3 or 4 months. A workable solution in this case is to acknowledge the 3-month mean patterns that have already demonstrated their authenticity through multiple independent consecutive appearances in the 1-month analysis results.

Table E1 characterizes the 3-month patterns as Table 2 did for the 1-month patterns. The reappearance of 1-month patterns in the 3-month results is a form of confirmation of the reality of those patterns. By comparing the strengths of the 1- and 3-month solutions

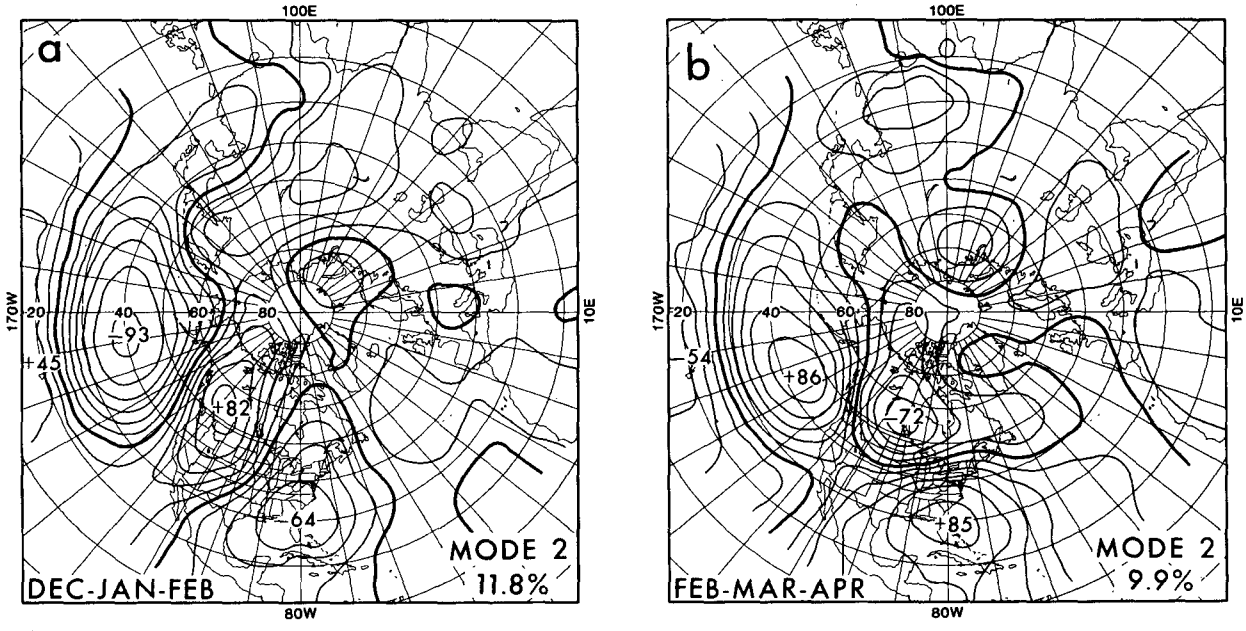

FIG. E1. The Pacific/North American pattern (PNA) in (a) December–January–February (mode 2; prototype) and in (b) February–March–April (mode 2), during which it is combined with the Tropical/Northern Hemisphere (TNH) pattern.

Unauthenticated | Downloaded 08/21/22 12:56 PM UTC

we also note which averaging period has better defined interannual variance for the given pattern. Results of this comparison are not expected to coincide closely with the intermonthly versus interannual strength dichotomy in E, but do provide supplementary information.

In the seasonal results, the PNA and TNH patterns blend in two periods (JFM and FMA; see Fig. E1a for a "pure" PNA, E1b for a PNA/TNH blend), when they are separately strong in the one-month analyses, and the EP is absorbed into the WPO in all but one season (hence it is no longer listed). A possible explanation for this blending is that in some winters both patterns may be more likely than usual to occur (perhaps because of convective activity in the equatorial Pacific; Mo and Livezey, 1986). If their typical lifetimes are considerably shorter than three months (which experience suggests is true) they will appear as independent modes in 1-month mean data but in the same mode in 3-month mean data. The NAO not only continues to appear each season, but occupies stronger mode numbers than in the 1-month solutions. In E, the West Atlantic Pattern, which contains much of our NAO, has a stronger intermonthly than interannual signal, but the Zonally Symmetric signal, also containing NAO, has most of its strength at the interannual time scale. In general, our seasonal results contain more superimpostions of patterns and more instances of deviations from the pattern prototypes defined using 1-month results. In most cases the deviations are erratic, but for some patterns they are consistent, in which case the 3-month pattern prototype is redefined. For example, the 3-month WPO is farther east (barely west of the mid-Pacific) in the 3-month solutions, because it incorporates what would be the EP in the monthly solutions. The two eastern centers of EU2 appear 10° farther east than in the 1-month results. For the EU1 pattern, there is no appreciable strength difference between our 1- and 3-month solutions, whereas it shows a stronger signal on the interannual than intermonthly time scales in E. The NP no longer has a pair of like-signed centers, but rather a giant single anomaly band which moves farther south in summer than in the 1-month results. The PT loses its integrity, showing only one good seasonal period. This is hardly surprising because the month-to-month changes in its form are greater than those of any other pattern. The SZ acquires a more coherent active period and assumes more dominant mode numbers. Figure E2 shows the 3-month SZ pattern for July–August–September.

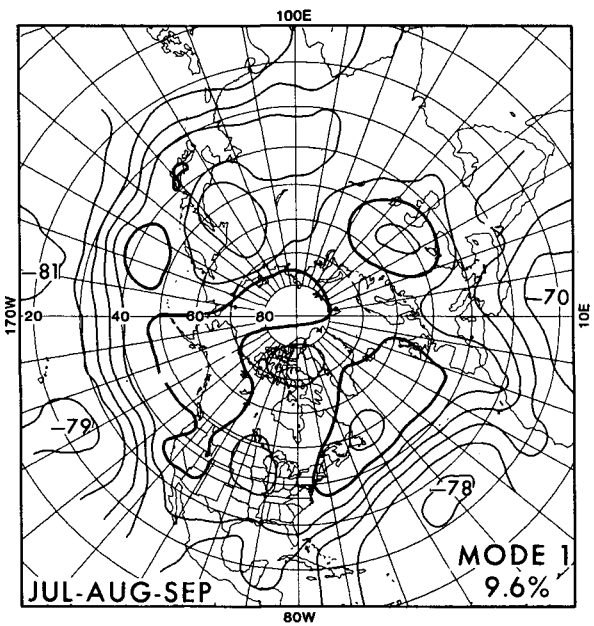

FIG. E2. The Subtropical Zonal pattern (SZ) in July–August–September (mode 1; prototype).

The RPCA was applied also to 2-month mean 700 mb heights. Although no results are shown here, they show a high degree of continuity with the 1- and 3-month results, never producing features differing significantly from either adjacent averaging period.

Unauthenticated | Downloaded 08/21/22 12:56 PM UTC

APPENDIX F

Principal Component Time Series for Some Prominent Circulation Patterns in Selected Months
Values Are standardized and multiplied by 100.

	NAO					PNA					
Year	Dec*	Jan	Feb	Mar	Jul	Dec*	Jan	Feb	Mar	Apr	Year
1950	−35	8	8	−54	112	−185	−197	−33	46	114	1950
1951	132	−89	48	207	−116	40	−5	−110	−19	−15	1951
1952	−112	−101	11	124	−77	−177	−163	6	−152	193	1952
1953	143	14	28	−4	−7	19	75	−4	−63	47	1953
1954	−197	−75	21	−73	−25	49	−106	−6	−40	−77	1954
1955	−62	104	192	39	−262	117	40	−178	−37	−35	1955
1956	63	6	47	−131	154	18	−185	−135	9	2	1956
1957	−111	−140	109	118	111	13	−75	−76	30	−41	1957
1958	−44	20	56	221	169	51	105	132	−55	4	1958
1959	55	92	−256	−162	−65	131	−119	−95	58	42	1959
1960	2	84	163	−19	89	116	40	26	105	113	1960
1961	−42	−66	−170	33	32	111	108	−21	79	−57	1961
1962	155	−117	−42	248	202	−94	−26	2	−58	98	1962
1963	8	185	95	−109	−16	109	114	161	−149	−60	1963
1964	−1	64	−52	−74	−230	166	67	44	−177	−159	1964
1965	−7	−58	21	−13	36	−168	14	−98	−52	−29	1965
1966	72	129	151	46	−101	−71	76	−179	46	−123	1966
1967	25	85	−86	−107	−14	13	6	−18	−87	−195	1967
1968	77	−21	17	−41	62	−121	−112	256	80	−30	1968
1969	55	154	108	46	−24	−10	−162	−49	33	172	1969
1970	97	146	90	88	−22	129	20	91	21	−121	1970
1971	10	53	−55	15	31	−70	−120	8	49	134	1971
1972	−121	−67	−45	−13	3	−174	0	−50	173	22	1972
1973	−212	−50	−17	1	−33	−67	34	32	−178	−106	1973
1974	35	−144	−3	−128	27	40	−12	−17	58	54	1974
1975	−76	−49	−121	−32	−49	−6	−17	−33	21	−132	1975
1976	−88	−15	−134	−126	58	75	62	−84	−31	104	1976
1977	112	93	126	36	12	25	198	132	−144	35	1977
1978	−4	−90	105	−114	135	−18	84	143	81	−4	1978
1979	167	100	9	−1	−25	−135	36	−134	−11	−161	1979
1980	−112	82	−101	−22	66	106	−28	138	−84	194	1980
1981	−31	−107	−23	74	−51	139	212	17	151	−56	1981
1982	203	99	−127	−121	−85	−29	−73	−32	−76	10	1982
1983	−113	−102	−92	46	−133	−48	43	138	273	−9	1983
1984	−42	−229	−79	1	35	−90	65	26	99	70	1984

* November and December values are for previous calendar year.
Note: The signs of the principal components are in accordance with the following eigenvector pattern polarities:
NAO—Greenland/Davis Strait center is positive.
PNA—Western North American center is positive.
WPO—Kamchatka/northwest Atlantic center is positive.
TNH—U.S. Great Lakes/Hudson Bay center is negative.

Unauthenticated | Downloaded 08/21/22 12:56 PM UTC

APPENDIX F (*Continued*)

	WPO				TNH		
Year	Nov*	Dec*	Jan	Feb	Jan	Feb	Year
1950	—	19	4	27	145	10	1950
1951	299	91	−56	43	35	−114	1951
1952	−7	16	−117	−84	8	−50	1952
1953	−59	−106	78	−175	40	158	1953
1954	−88	−106	21	35	−41	28	1954
1955	−10	143	−112	36	52	−15	1955
1956	97	212	101	125	−286	71	1956
1957	19	101	−3	96	123	100	1957
1958	−28	0	−102	53	−133	−112	1958
1959	11	2	3	−157	−17	8	1959
1960	−2	−79	−41	−93	−0	−37	1960
1961	−2	−61	28	112	−40	−112	1961
1962	−42	116	144	−61	75	10	1962
1963	−147	89	319	137	133	165	1963
1964	−25	−115	−77	−108	5	177	1964
1965	120	116	13	46	11	59	1965
1966	101	−33	−70	−132	−54	2	1966
1967	182	−45	−90	−77	41	107	1967
1968	−25	−23	83	186	−110	5	1968
1969	−119	110	−54	−57	−168	−311	1969
1970	−33	−176	89	−70	28	40	1970
1971	189	−71	129	100	48	2	1971
1972	−34	−63	−80	230	173	−31	1972
1973	−93	23	−22	−158	−73	−93	1973
1974	122	−125	147	46	69	50	1974
1975	−27	−127	−154	−71	133	111	1975
1976	−4	37	−59	20	67	25	1976
1977	−121	−23	−50	−92	33	108	1977
1978	0	103	46	−49	−85	−27	1978
1979	117	−72	−108	65	17	−42	1979
1980	51	63	62	−51	−51	−33	1980
1981	−92	197	93	2	−190	−42	1981
1982	−60	−44	−43	122	103	75	1982
1983	−19	−185	−166	−57	−116	−193	1983
1984	−141	14	44	4	27	−97	1984

Unauthenticated | Downloaded 08/21/22 12:56 PM UTC

REFERENCES

Blackmon, M. L., Y. H. Lee and J. M. Wallace, 1984a: Horizontal structure of 500 mb height fluctuations with long, intermediate and short time scales. *J. Atmos. Sci.*, **41,** 961–979.

——, ——, —— and H. H. Hsu, 1984b: Time variation of 500 mb height fluctuations with long, intermediate and short time scales as deduced from lag-correlation statistics. *J. Atmos. Sci.*, **41,** 981–991.

Esbensen, S. K., 1984: A comparison of intermonthly and interannual teleconnections in the 700 mb geopotential height field during the Northern Hemisphere winter. *Mon. Wea. Rev.*, **112,** 2016–2032.

Guttman, L., 1954: Some necessary conditions for common-factor analysis. *Psychometrika,* **19,** 149–161.

Harris, C. W., and H. F. Kaiser, 1964: Oblique factor analytic solutions by orthogonal transformations. *Psychometrika,* **29,** 347–362.

Horel, J. D., 1981: A rotated principal component analysis of the interannual variability of the Northern Hemisphere 500 mb height field. *Mon. Wea. Rev.*, **109,** 2080–2092.

——, 1984: Complex principal component analysis: Theory and examples. *J. Climate Appl. Meteor.*, **23,** 1660–1673.

Hsu, H., and J. M. Wallace, 1985: Vertical structure of wintertime teleconnection patterns. *J. Atmos. Sci.*, **42,** 1693–1710.

Kaiser, H. F., 1958: The Varimax criterion for analytic rotation in factor analysis. *Psychometrika,* **23,** 187–200.

——, 1959: Computer program for Varimax rotation in factor analysis. *Educ. Psych. Meas.*, **19,** 413–420.

Karl, T. R., A. J. Koscielny and H. F. Diaz, 1982: Potential errors in the application of principal component (eigenvector) analysis to geophysical data. *J. Appl. Meteor.*, **21,** 1183–1186.

Klein, W. H., 1983: Objective specification of monthly mean surface temperature from mean 700 mb heights. *Mon. Wea. Rev.*, **111,** 674–691.

——, and J. E. Walsh, 1983: A comparison of point-wise screening and empirical orthogonal functions in specifying monthly surface temperatures from 700 mb data. *Mon. Wea. Rev.*, **111,** 669–673.

Lebow, W. M., and P. M. Toldalagi, 1985: Long-range prediction of 700 mb data through the group method of data handling. Final Report, NWS Contract NA83AA-9-00005. [Available at Scientific Systems, Inc., 54 Rindge Av. Ext., Cambridge, MA. 02140.]

Livezey, R. E., and W. Y. Chen, 1983: Statistical field significance and its determination by Monte Carlo techniques. *Mon. Wea. Rev.*, **111,** 46–59.

Mo, K. C., and R. E. Livezey, 1986: Tropical–extratropical geopotential height teleconnections during the Northern Hemisphere winter. *Mon. Wea. Rev.*, **114,** 2488–2515.

Namias, J., 1981: Teleconnections of 700 mb height anomalies for the Northern Hemisphere. *Calcofi Atlas No. 29.*

North, G. R., T. L. Bell, R. F. Cahalan and F. J. Moeng, 1982: Sampling errors in the estimation of empirical orthogonal functions. *Mon. Wea. Rev.*, **110,** 699–706.

O'Connor, J. F., 1969: Hemispheric teleconnections of mean circulation anomalies at 700 millibars. ESSA Tech. Rep. WB10, 103 pp.

Panofsky, H. A., and G. W. Brier, 1968: *Some Applications of Statistics to Meteorology.* The Pennsylvania State University, 224 pp.

Richman, M. B., 1986: Rotation of principal components. *J. Climatol.*, **6,** 293–335.

——, and P. J. Lamb, 1985: Climatic pattern analysis of three- and seven-day rainfall in the central United States: Some methodological considerations and a regionalization. *J. Climate Appl. Meteor.*, **24,** 1325–1343.

Thiebaux, H. J., and F. W. Zwiers, 1984: The interpretation and estimation of effective sample size. *J. Climate Appl. Meteor.*, **23,** 800–811.

van den Dool, H. M., and R. E. Livezey, 1984: Geographical distribution and seasonality of month-to-month correlation of monthly mean 700 mb heights. *Mon. Wea. Rev.*, **112,** 610–615.

Wallace, J. M., and D. S. Gutzler, 1981: Teleconnections in the geopotential height field during the Northern Hemisphere winter. *Mon. Wea. Rev.*, **109,** 784–812.

Walsh, J. E., 1984: Forecasts of monthly 700 mb height: Verification and specification experiments. *Mon. Wea. Rev.*, **112,** 2135–2147.

Unauthenticated | Downloaded 08/21/22 12:56 PM UTC